KIF17 stabilizes microtubules and contributes to epithelial morphogenesis by acting at MT plus ends with EB1 and APC

Fanny Jaulin and Geri Kreitzer

Department of Cell and Developmental Biology, Weill Cornell Medical College of Cornell University, New York, NY 10021

Epithelial polarization is associated with selective stabilization and reorganization of microtubule (MT) arrays. However, upstream events and downstream consequences of MT stabilization during epithelial morphogenesis are still unclear. We show that the anterograde kinesin KIF17 localizes to MT plus ends, stabilizes MTs, and affects epithelial architecture. Targeting of KIF17 to plus ends of growing MTs requires kinesin motor activity and interaction with EB1. In turn, KIF17 participates in localizing adenomatous polyposis coli (APC) to the plus ends of a subset of MTs. We found that KIF17 affects MT dynamics, polymerization rates, and MT plus end stabilization to generate posttranslationally acetylated MTs. Depletion of KIF17 from cells growing in three-dimensional matrices results in aberrant epithelial cysts that fail to generate a single central lumen and to polarize apical markers. These findings implicate KIF17 in MT stabilization events that contribute to epithelial polarization and morphogenesis.

Introduction

Remodeling of microtubules (MTs) accompanies polarization during numerous events including cell differentiation, division, and migration. In epithelial cells, reorganization of MT arrays is associated with the formation of structurally and functionally polarized apical and basolateral membrane domains during differentiation (Müsch, 2004). In nonpolarized epithelial cells, MTs radiate from the centrosome, whereas after polarization, many MTs become noncentrosomal, stabilized, and enriched in posttranslationally modified tubulin (Bré et al., 1987; Bacallao et al., 1989; Pepperkok et al., 1990; Jaulin et al., 2007). Although signaling pathways involved in apico-basolateral polarization have emerged, the molecular events underlying generation of stable MT arrays in epithelia and their contribution to epithelial morphogenesis are still unclear.

In epithelia, cell–cell adhesion and cadherin engagement trigger changes in MT dynamics that result in the stabilization of a subset of MTs (Chausovsky et al., 2000; Waterman-Storer et al., 2000). The kinase Par1 regulates MT stabilization

and reorganization (Cox et al., 2001; Doerflinger et al., 2003; Cohen et al., 2004), in part, by modulating cadherin association with the cortical actin cytoskeleton (Elbert et al., 2006). Furthermore, the tumor suppressor adenomatous polyposis coli (APC) and the plakin ACF-7, both important cytoskeletal organizers in epithelial cells, associate with MT plus ends and contribute to MT stabilization (Kodama et al., 2003; Kita et al., 2006; Kroboth et al., 2007). MTs are stabilized by factors that dampen dynamics (Galjart, 2005) or cap, in an ATP-dependent manner, MT plus ends, extending their half-life by preventing addition and loss of tubulin subunits (Infante et al., 2000). Stabilization results in accumulation of posttranslationally modified forms of tubulin in MTs (Verhey and Gaertig, 2007). These posttranslational modifications affect the activity of several kinesin family motors (Liao and Gundersen, 1998; Reed et al., 2006; Ikegami et al., 2007; Dunn et al., 2008; Konishi and Setou, 2009), which in turn can modify vesicular trafficking processes and the organization of organelles (Minin, 1997; Kreitzer et al., 1999; Lin et al., 2002). Thus, MT stabilization could contribute to the establishment and maintenance of asymmetry by defining a polarity

The Rockefeller University Press $30.00
J. Cell Biol. Vol. 190 No. 3 443–460
www.jcb.org/cgi/doi/10.1083/jcb.201006044

JCB 443

axis in cells for transport and targeted delivery of vesicles, protein complexes, and mRNA by MT-associated motors. Although MT stabilization is associated temporally with the generation of mature epithelial architecture, it is still not known whether this contributes directly to apico-basolateral polarization of epithelia.

MT plus end binding proteins (known as +TIPs) are key regulators of MT dynamics and organization. By associating selectively with growing MT ends, these +TIPs modulate MT dynamicity, polymerization, and plus end stabilization (Akhmanova and Steinmetz, 2008). End-binding protein 1 (EB1) and its yeast homologues, Bim1 and Mal3, promote the addition of tubulin subunits to MTs and associate with MT plus ends by recognizing structural features of growing MT tips (Sandblad et al., 2006; Bieling et al., 2007; Vitre et al., 2008; Dixit et al., 2009). EB1 forms the core machinery for MT tip tracking in eukaryotes and targets additional +TIPs to MT ends (Akhmanova and Steinmetz, 2008). MT tip tracking can occur by three mechanisms: treadmilling, hitchhiking, and kinesin-mediated transport. In metazoa, the treadmilling proteins CLIP170 and p150^{Glued} contain Cap-Gly domains, and basic and serine-rich motifs that mediate interactions with the EB1 C terminus and tubulin, respectively, which facilitates treadmilling and potentially copolymerization at MT plus ends (Diamantopoulos et al., 1999; Ligon et al., 2003; Folker et al., 2005; Dixit et al., 2009). Other +TIPs, including APC and ACF-7, are instead thought to track MT ends by hitchhiking on EB1 (Mimori-Kiyosue et al., 2000a; Slep et al., 2005). A conserved motif in these proteins, Ser-X-Ile-Pro (SXIP), mediates their interaction with a hydrophobic cavity in EB1 and thus association with MT plus ends (Honnappa et al., 2009). In fungi, anterograde kinesins Tea2 (*Schizosaccharomyces pombe*), Kip2 (*Saccharomyces cerevisiae*), and KipA (*Aspergillus nidulans*) also track MT plus ends and mediate transport of additional +TIPs, including homologues of metazoan treadmilling and hitchhiking proteins (Browning et al., 2003; Busch et al., 2004; Carvalho et al., 2004; Konzack et al., 2005). Furthermore, Tea2 in fission yeast interacts with and is targeted to MT plus ends by EB1 (Mal3; Browning et al., 2003). By transporting MT regulators at plus ends, these kinesins modulate MT organization, stabilization, and cell polarization. Whether anterograde kinesins contribute to MT tip tracking in metazoa, and whether this affects MT stabilization, organization, and cell polarization, is still a matter of debate, as no examples have been reported (Wu et al., 2006).

We show here that the kinesin-2 family protein KIF17 localizes to MT plus ends and is enriched at the ends of a subset of MTs. KIF17 interacts with two other +TIPs: EB1 and APC. Interaction between EB1 and the motor domain of KIF17 targets KIF17 to MT plus ends. KIF17 binds APC, independently of EB1, and contributes to its localization at MT ends. In functional assays, KIF17 dampens MT dynamics, slows MT polymerization, and promotes MT plus end capping, resulting in MT stabilization. Furthermore, depletion of KIF17 from epithelial cells grown in 3D matrices inhibits apical polarization and epithelial morphogenesis. Together, our results provide evidence that anterograde kinesins associate with MT plus ends and contribute to MT stabilization events associated with polarization of epithelial cells.

Results

KIF17 colocalizes with EB1 at MT plus ends in epithelial cells

We analyzed the distribution of kinesin family proteins during epithelial polarization and found that KIF17, unlike other anterograde kinesins, often localized at the distal ends of MTs in epithelial cells (Fig. 1 A). In Caco2 and MDCK cells, KIF17 also localized in the nucleus, cytoplasm, and along MTs. The nuclear pool of KIF17 was expected based on the presence of a C-terminal nuclear localization signal. Cytosolic KIF17 likely represents an inactive pool of the motor (see the following sections). MT-associated KIF17 was obvious at high magnification and detected prominently at MT plus ends (Fig. 1 A, boxed regions).

Quantitative colocalization analysis revealed that KIF17 colocalizes with 62% and 38% of EB1-labeled MT ends in Caco2 and MDCK cells, respectively (Fig. 1, B and D). Interestingly, KIF17 localizes as discrete puncta at the head of EB1 comets (Fig. 1 C, arrows) rather than in comet-like structures characteristic of +TIP treadmilling proteins. In some cases, we also saw smaller puncta along the comet tail (Fig. 1 C, arrowheads). MDCK cells exhibit protruding membrane structures where MTs often converge (Näthke et al., 1996). These were described as regions of active membrane extension but their functional significance is not known. Analysis of KIF17-EB1 colocalization in these regions revealed a 1.9-fold enrichment (72% vs. 38%) of KIF17 on EB1-labeled MTs in cell extensions as compared with all EB1-labeled MTs (Fig. 1 D). Preincubation of KIF17 antibody with immunogenic peptide (blocking peptide) reduced the amount of KIF17 detected by immunofluorescence and immunoblotting to background levels (Figs. 1 D and S1, A and B). Colocalization with EB1 at MT ends is not a general property of anterograde kinesins, as neither KIF5 nor KIF3 colocalized with EB1 (unpublished data).

KIF17 interacts with EB1 via the kinesin motor domain

To determine if endogenous KIF17 and EB1 interact, we incubated epithelial cell lysates with antibodies to KIF17 or the closely related kinesin-2 family member, KIF3. Immunoblotting revealed that EB1 coprecipitates with KIF17 but not with KIF3 (Fig. 2 A). We mapped the interaction between KIF17 and EB1 using constructs encoding full-length (KIF17-FL and EB1-FL), truncated, or mutant (KIF17-M, KIF17-S, KIF17-T, EB1-N, EB1-C, EB1Δ7, EB1-FL^{EE}, and EB1-C^{EE}) human KIF17 and EB1 (Fig. 2 B). We transfected MDCK cells with myc-tagged KIF17 and GFP-tagged EB1, and incubated lysates with myc antibodies. Immunoblotting with GFP antibody revealed that EB1-FL and EB1-C, but not EB1-N, coprecipitated with KIF17-FL and KIF17-M (Fig. 2 C). Thus, the motor domain of KIF17 interacts with the C terminus of EB1. Interaction of EB1 with KIF17 is selective, as neither KIF5B motor domain nor full-length KIF3A, KIF4, or KIF9 are pulled down by GST-EB1-FL (Fig. S1, C and D). Furthermore, purified HA-KIF17-FL bound in vitro to GST-tagged EB1-FL and EB1-C (Fig. 2 D). The weak binding detected between EB1-N
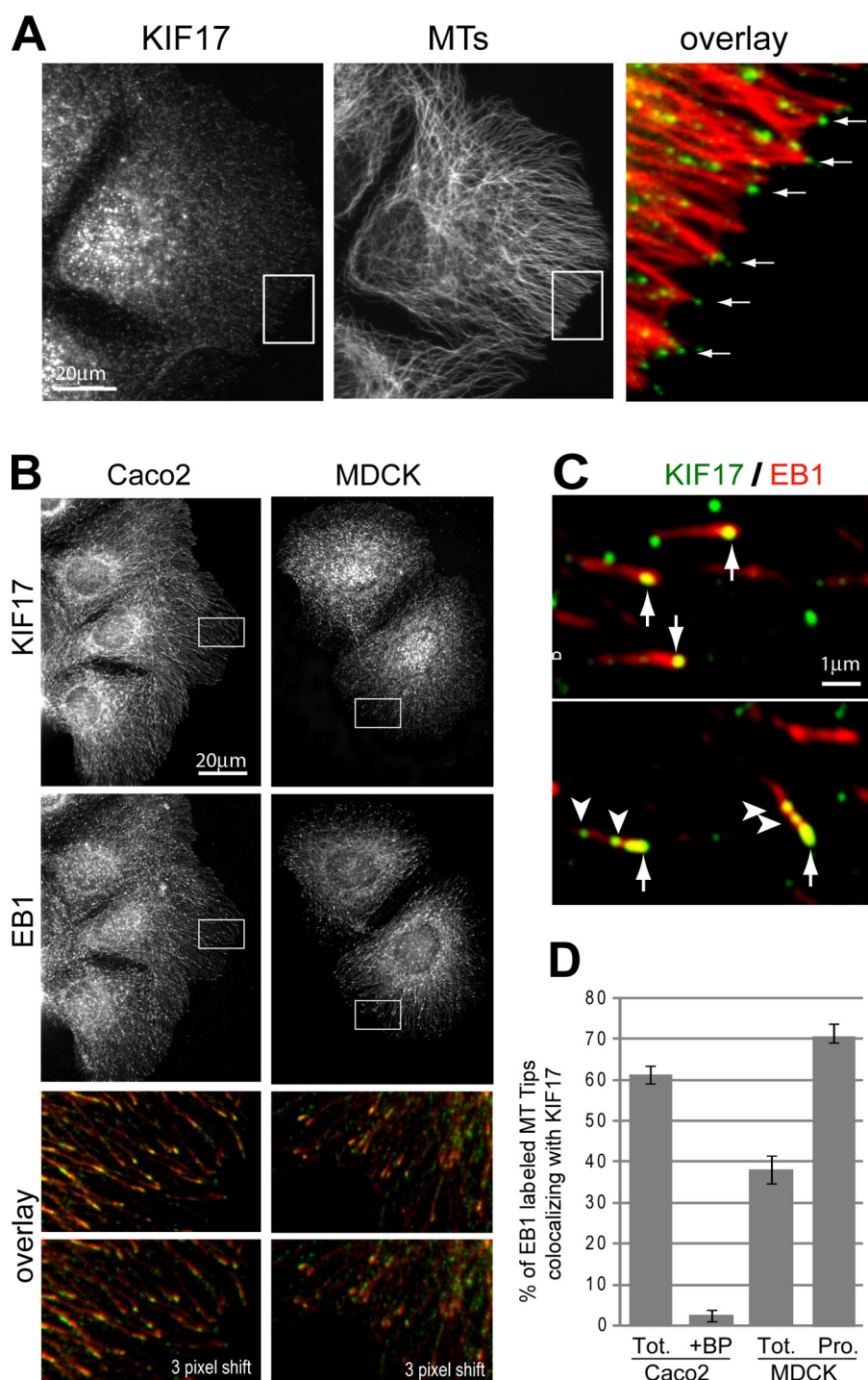
A KIF17 | MTs | overlay

B Caco2 | MDCK — KIF17 / EB1 / overlay (3 pixel shift)

C KIF17 / EB1

D

Figure 1. **KIF17 colocalizes with EB1 at MT plus ends.** (A) Immunostaining of tyrosinated α-tubulin and KIF17 in Caco2 cells. Color overlay: enlargement of boxed regions showing KIF17 (green) at the plus ends of MTs (red, see arrows). (B) Immunostaining of KIF17 and EB1 in Caco2 and MDCK cells. Overlay panels show magnifications of EB1 (red) and KIF17 (green) from the boxed regions. In the bottom overlay panels, the KIF17 image was shifted 3 pixels to highlight the coincident staining pattern. (C) High-magnification images of EB1 and KIF17 in Caco2 cells. Arrows, KIF17 puncta at the head of EB1 comets; arrowheads, KIF17 puncta along the EB1 tail. (D) Quantification of KIF17 colocalization with EB1-labeled MTs in Caco2 ($n = 4{,}575$) and MDCK ($n = 2{,}622$) cells (n = the number of EB1-labeled MT ends analyzed in at least three experiments). Random colocalization was determined and subtracted from each dataset as described in Material and methods. +BP, analysis after preincubation of KIF17 IgG with immunogenic peptide ($n = 1{,}203$); Tot., total EB1-labeled MTs throughout entire cell ($n = 2{,}622$); Pro., EB1-labeled MTs in cell protrusions ($n = 231$). Error bars indicate SEM.

(containing the MT binding site) and KIF17-FL likely reflects background binding levels (perhaps due to the presence of tubulin in reticulocyte lysates). KIF17 and EB1 also coimmunoprecipitated from cells treated with the MT antagonist nocodazole (NZ; Fig. S1 E). These data show that KIF17 and EB1 can interact directly and independently of MTs.

The EB1 C terminus interacts with proteins that act as allosteric activators of EB1 tip tracking (e.g., CLIP170 and p150[glued]) and with proteins that hitchhike on EB1, such as APC. To determine if KIF17 falls into either of these groups, we transfected MDCK cells with GFP-EB1 mutants with reduced binding to allosteric activators (EB1Δ7, 7-aa deletion; Bu and Su, 2003; Hayashi et al., 2005; Komarova et al., 2005) or hitchhikers (EB1-C[E211/E213]; Wen et al., 2004; Slep et al., 2005), and examined binding to GST-KIF17-M. EB1Δ7 was pulled down by KIF17-M as efficiently as EB1-FL, but pull-down of EB1-C[E211/E213] was reduced significantly compared with EB1-C (Fig. 2 E). This suggests that KIF17 is not an allosteric activator of EB1 but may be targeted to MT plus ends by EB1.

Several EB1 hitchhikers contain a conserved SXIP motif needed for binding to EB1 and association with MT tips (Honnappa et al., 2009). The KIF17 motor domain does not have an
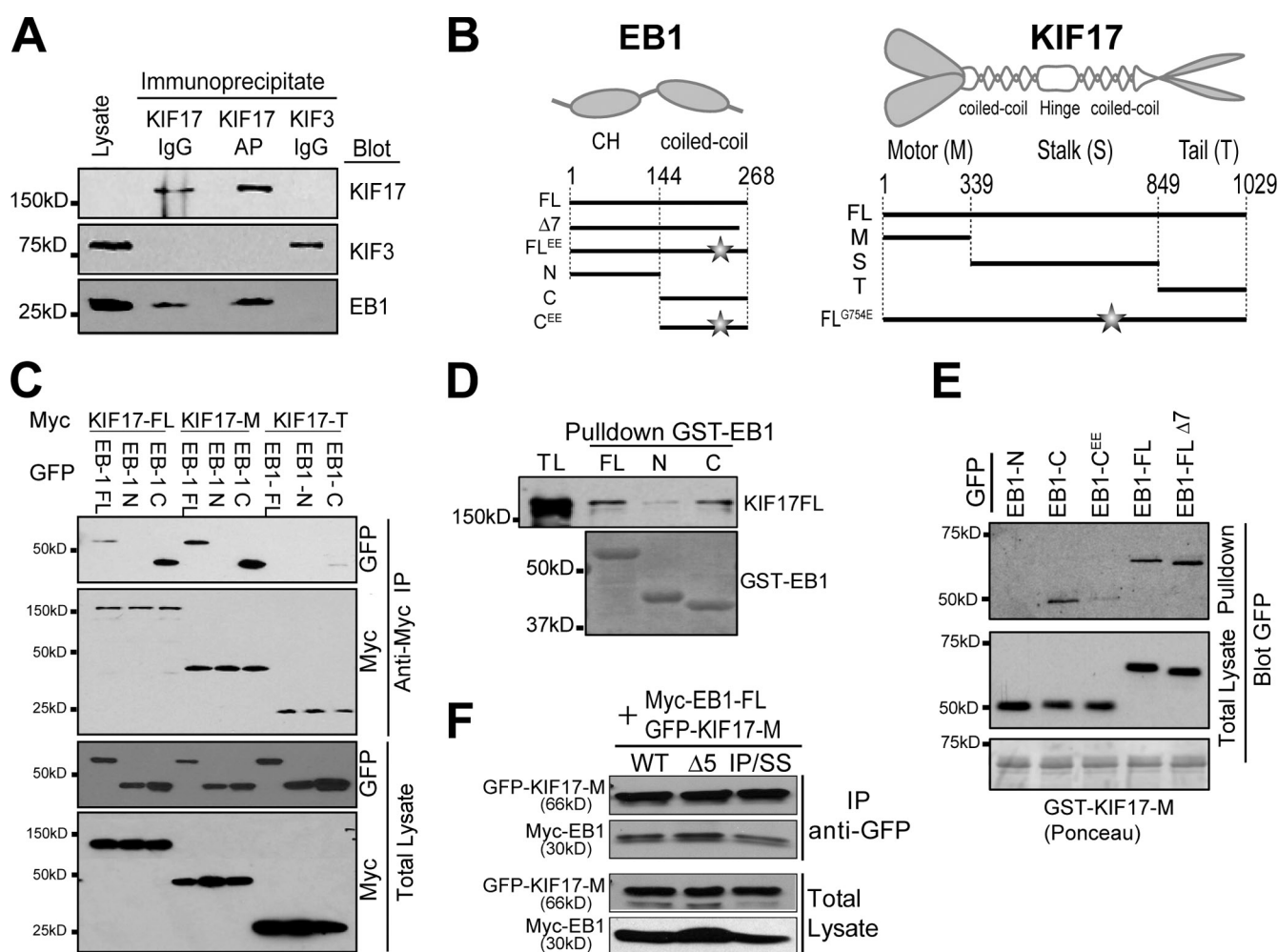
Figure 2. **KIF17 motor domain interacts with EB1.** (A) Immunoprecipitation of endogenous KIF17 or KIF3 from HEK-293 cells (AP, affinity purified IgG). Western blots probed for KIF17, KIF3A, or EB1. 1/20 volume used for immunoprecipitation was loaded for total lysates. At this concentration, KIF17 is not detected. (B) Schematic diagram of EB1 and KIF17 constructs. Numbers indicate amino acid position. (C) Immunoprecipitation of myc-tagged KIF17-FL, KIF17-M, or KIF17-T from MDCK cells cotransfected with GFP-tagged EB1-FL, EB1-N, or EB1-C. Immunoprecipitates and total lysates were blotted with anti-myc and anti-GFP antibodies. (D) Binding of in vitro translated HA-KIF17-FL to purified GST-tagged EB1-FL (FL), EB1-C (C), or EB1-N (N). TL, total lysate. (E) Pull-down of GFP-tagged EB1 constructs expressed in MDCK cells by purified GST-KIF17-M. (F) Coimmunoprecipitation of myc-EB1-FL and GFP-KIF17-M, GFP-KIF17-M^{IP}, or GFP-KIF17-MΔ5 from MDCK lysates.

SXIP motif but does contain a GIIP motif at amino acids 112–115. We substituted this immunoprecipitation motif with two serines (KIF17-M^{IP}). Binding of GFP-KIF17-M^{IP} to myc-EB1-FL was not affected as compared with GFP-KIF17-M (Fig. 2 F). In S. *pombe*, the kinesin Tea2 also lacks a SXIP motif but interacts with EB1 (Mal3) via an N-terminal extension preceding the motor domain (Browning and Hackney, 2005). Deletion of the five amino acids N terminal to the predicted KIF17 motor domain (KIF17-MΔ5) did not affect its binding to EB1 (Fig. 2 F). Together, these results suggest a nonclassical interaction between EB1 and KIF17.

EB1 targets KIF17 to MT plus ends

To test if EB1 affects the distribution of KIF17 on MTs, we overexpressed myc-EB1-FL in Caco2 cells. Myc-EB1-FL localized along the length of MTs and increased KIF17 localized along the MT lattice (Fig. 3 A). This likely represents recruitment of KIF17 from the cytoplasm because its protein levels were unchanged (unpublished data). Overexpressed myc-EB1-FL$^{E211/E213}$ also

localized along MTs but did not recruit KIF17 to MTs, as expected from its reduced interaction with KIF17 (Fig. 2 E). Line-scan analysis of KIF17 immunofluorescence along the most peripheral 10 µm of MTs showed that expression of EB1-FL increased the number and intensity of KIF17 puncta on MTs by 1.7- and 4.4-fold, respectively, as compared with EB1-FL$^{E211/E213}$ (Fig. 3 B). Depletion of EB1 by 75–80% with siRNA reduced the number of MTs with KIF17 puncta at their plus ends by 80% but did not alter MT arrays noticeably (Fig. 3 C). Conversely, KIF17 depletion had no detectable effect on localization of endogenous EB1 at MT plus ends (Fig. 3 D). Thus, EB1 is required for MT plus end localization of KIF17 but KIF17 is not required for plus end localization of EB1.

Kinesin motor activity is required for KIF17 association with MT plus ends

To study KIF17 in living cells, we microinjected cDNA encoding GFP tagged full-length KIF17 (GFP-KIF17-FL) and monitored
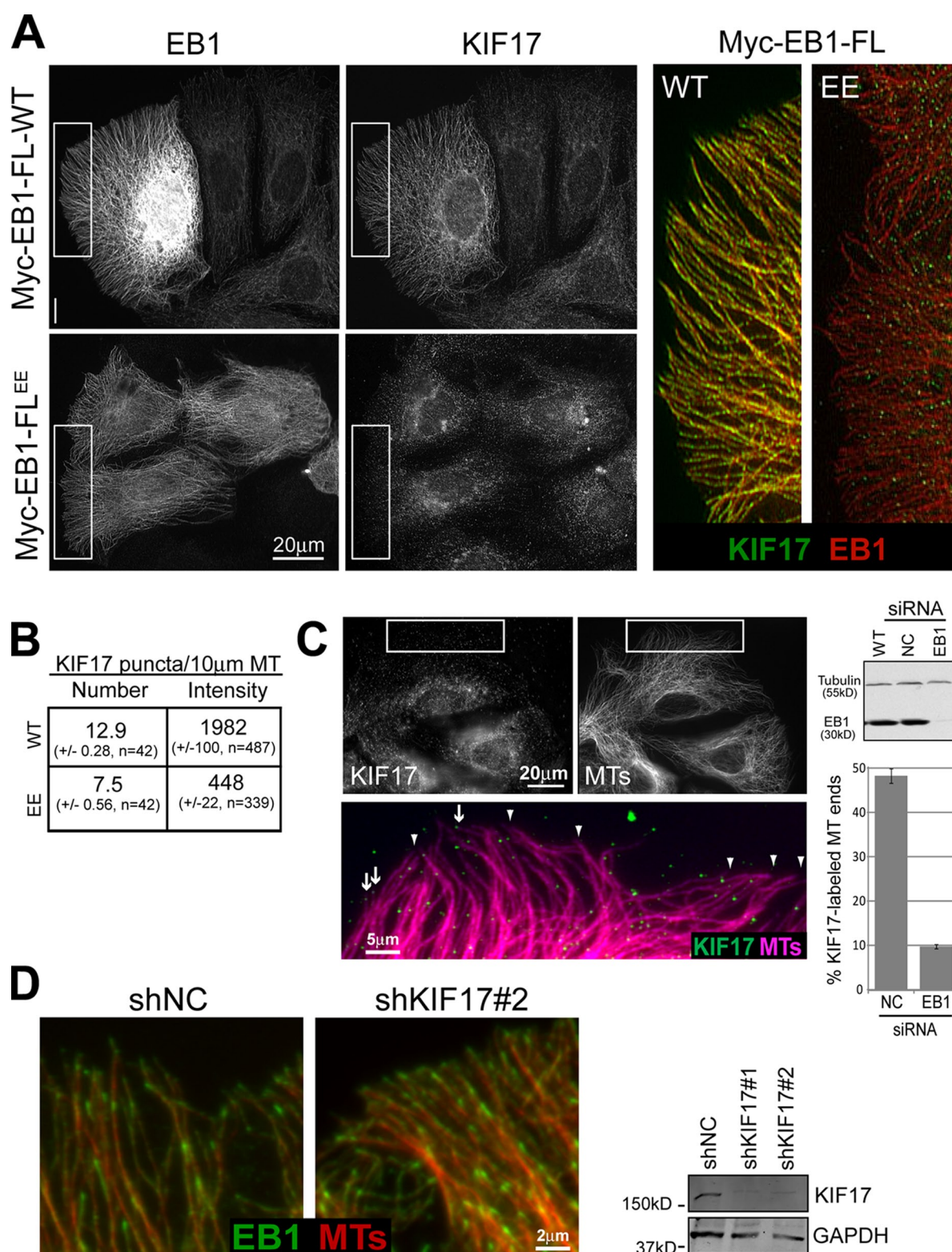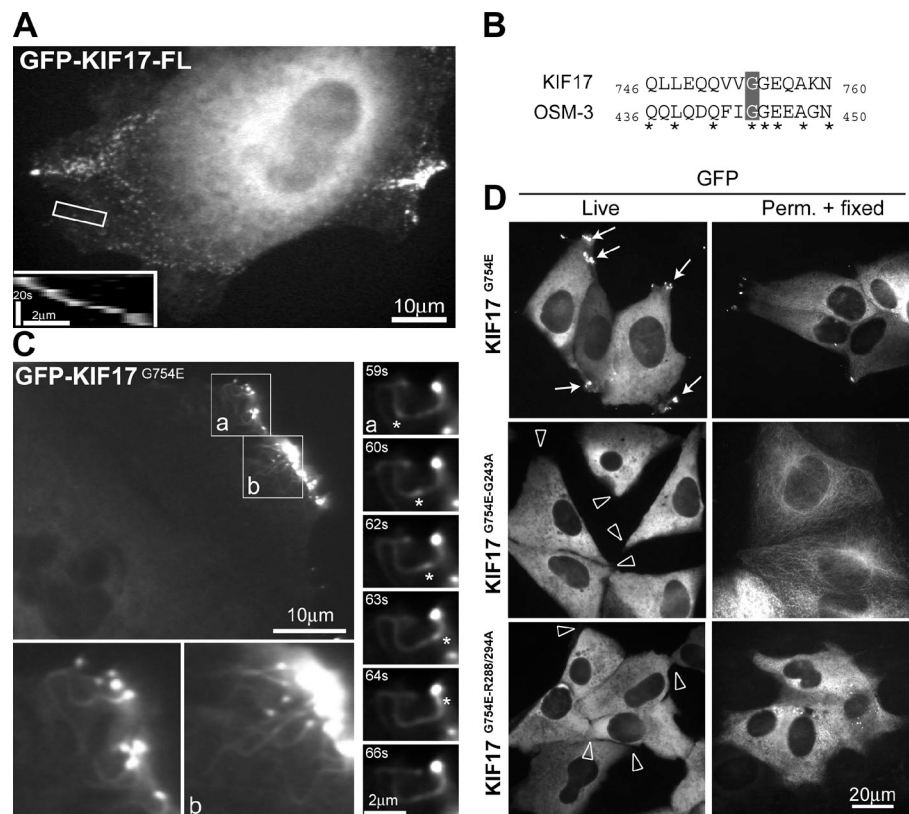
Figure 3. EB1 targets KIF17 to MTs. (A) Immunostaining of endogenous KIF17 and transfected myc-EB1-FL or myc-EB1-FL^EE in Caco2 cells. Color overlays show boxed regions at higher magnification. (B) Line-scan analysis of the number and fluorescence intensity of KIF17 puncta along the distal 10 µM of individual MTs in cells expressing myc-EB1-FL or myc-EB1-FL^EE. Data derived from three experiments in which 487 and 339 puncta along 42 MTs were analyzed in cells expressing myc-EB1 wild-type (WT) or mutant (EE) proteins. (C) Immunostaining of KIF17 and tyrosinated MTs in EB1-depleted cells. Color overlay shows an enlargement of the boxed regions. Arrows, MT ends decorated by KIF17; arrowheads, MT ends not decorated by KIF17. Western blot shows EB1 and tubulin levels in siNC or siEB1 transfected cells. Graph shows quantification of MT ends decorated by KIF17 in siNC or siEB1 cells (n = 3,058 and n = 3,882, respectively, compiled from three experiments). Error bars indicate SEM. (D) Immunostaining of tyrosinated MTs and EB1 in control and KIF17-depleted cells. Western blot shows KIF17 and glyceraldehyde 3-phosphate dehydrogenase (GAPDH) levels in Caco2 cells infected with lentiviral control (shNC) or KIF17 shRNAs (shKIF17#1 and shKIF17#2 target two unique sequences).

Figure 4. **Association of GFP-KIF17^{G754E} with MT plus ends requires kinesin ATPase and MT-binding activities.** (A) Single frame from a time-lapse recording of MDCK cells expressing GFP-KIF17-FL. Inset shows a kymograph of a moving GFP-KIF17-FL puncta during 20 s of the time-lapse recording (Video 1). The inset shows an enlargement of the boxed region. (B) Alignment of the hinge regions of *C. elegans* OSM-3 and human KIF17. The gray box shows the position of the G-to-E mutations in KIF17 and OSM-3. Numbers at left and right indicate amino acid position. Asterisks indicate sequence identities between KIF17 and OSM-3. (C) Single frame from a time-lapse recording of Caco2 cells injected with GFP-KIF17^{G754E} cDNA (Video 2). Boxed regions (a and b) are enlarged in the bottom panels. (B, right) Selected frames from the time-lapse recording. Asterisks indicate a KIF17 puncta moving on MTs toward the plus end. (D) Images of GFP-KIF17^{G754E}, GFP-KIF17$^{G754E-G243A}$, and GFP-KIF17$^{G754E-R288/294A}$ expressed by cDNA injection in live or prepermeabilized and fixed MDCK cells. GFP-KIF17^{G754E} localizes in cell extensions at MT ends (arrows), whereas GFP-KIF17$^{G754E-G243A}$ and GFP-KIF17$^{G754E-R288/294A}$ do not (arrowheads).

A — GFP-KIF17-FL — 20s / 2μm — 10μm

B
KIF17 $_{746}$ QLLEQQVV**G**GEQAKN $_{760}$
OSM-3 $_{436}$ QQLQDQFI**G**GEEAGN $_{450}$
         * * *   *** * *

C — GFP-KIF17^{G754E} — 10μm — 59s, 60s, 62s, 63s, 64s, 66s — 2μm

D — GFP
   Live | Perm. + fixed
   KIF17^{G754E}
   KIF17$^{G754E-G243A}$
   KIF17$^{G754E-R288/294A}$
   20μm

its behavior by time-lapse microscopy. When expressed at low levels, GFP-KIF17-FL puncta could be seen either moving along linear paths toward the cell periphery (Fig. 4 A and Video 1) or as relatively immobile spots at the cortex (Fig. 4 A). In many cells, GFP-KIF17-FL appeared primarily as diffuse cytoplasmic fluorescence, which suggests that a majority of overexpressed GFP-KIF17 is in an inactive state.

The activities of several kinesins, including the *Caenorhabditis elegans* homologue of KIF17 (OSM-3), are regulated by a conformational change involving autoinhibitory interaction of the kinesin tail and neck domains (Coy et al., 1999; Friedman and Vale, 1999; Lee et al., 2004; Imanishi et al., 2006). Substitution of glycine with glutamic acid at residue 444 in OSM-3 prevents tail/neck autoinhibition and results in a constitutively active mutant (Imanishi et al., 2006). We generated the corresponding mutation in KIF17 (KIF17-FL^{G754E}; Fig. 4 B). Sucrose gradient centrifugation of KIF17-FL and KIF17-FL^{G754E} in 0M and 1M NaCl showed that migration of KIF17-FL, but not KIF17-FL^{G754E}, in the gradient is salt sensitive (Fig. S1 G). This suggests that KIF17-FL^{G754E} is a conformationally extended mutant. In time-lapse recordings, we observed GFP-KIF17^{G754E} accumulating at MT plus ends (Fig. 4 C and Video 2). Like endogenous KIF17, GFP-KIF17^{G754E} localizes as discrete puncta rather than in comet-like structures at MT ends (Fig. 4 C, a and b) and in static clusters at the cortex near MT ends. In Caco2 cells, these cortical clusters localize randomly at the cell periphery, whereas in MDCK cells they are found at the tips of cell extensions (Fig. 4 D, top). We often observed smaller puncta of GFP-KIF17^{G754E} moving along MTs toward the plus ends and accumulating

there (Fig. 4 C, right; and Video 2). This suggests that GFP-KIF17^{G754E} moves along and accumulates at MT plus ends, although we cannot exclude direct recruitment to MT plus ends from the cytosol. After fixation, the MT-associated pool of KIF17 is lost and only the cortical pool remains.

We next generated point mutations in KIF17-FL and KIF17^{G754E} that abolish ATPase activity or MT binding. Kinesin mutants unable to bind or hydrolyze ATP interact with MTs but cannot move along the polymer, reflecting a "rigor" binding state. A point mutation in the γ-phosphate–sensing region of KIF17 (G243A) was reported to be a rigor mutant (KIF17^{G243A}; (Nakata and Hirokawa, 2003). Purified His-KIF17-M^{G243A} motor domain had negligible ATPase activity as compared with control His-KIF17-M (unpublished data). When expressed and visualized in living MDCK cells, KIF17$^{G754E-G243A}$ localized on MTs as expected, as well as in the cytoplasm, but did not accumulate at MT tips or in cell extensions. The MT-associated pool of rigor KIF17 was clearer in cells after mild permeabilization and fixation (Fig. 4 D). We also prepared KIF17-FL and KIF17^{G754E} double mutants (GFP-KIF17$^{R288/294A}$ and GFP-KIF17$^{G754E-R288/294A}$). By homology with kinesin-1 mutants (Woehlke et al., 1997), these are predicted to be deficient in MT binding. When expressed in MDCK cells, GFP-KIF17$^{G754E-R288/294A}$ did not localize along MTs or at MT plus ends but instead was cytoplasmic before and after fixation (Fig. 4 D). Interestingly, both KIF17-FL and KIF17^{G754E} rigor and MT-binding mutants coprecipitated with myc-EB1, which demonstrates that neither ATPase nor MT-binding activity are necessary for this interaction (Fig. S1 F). These data suggest that interaction with EB1 is not sufficient to target KIF17 to MT ends.
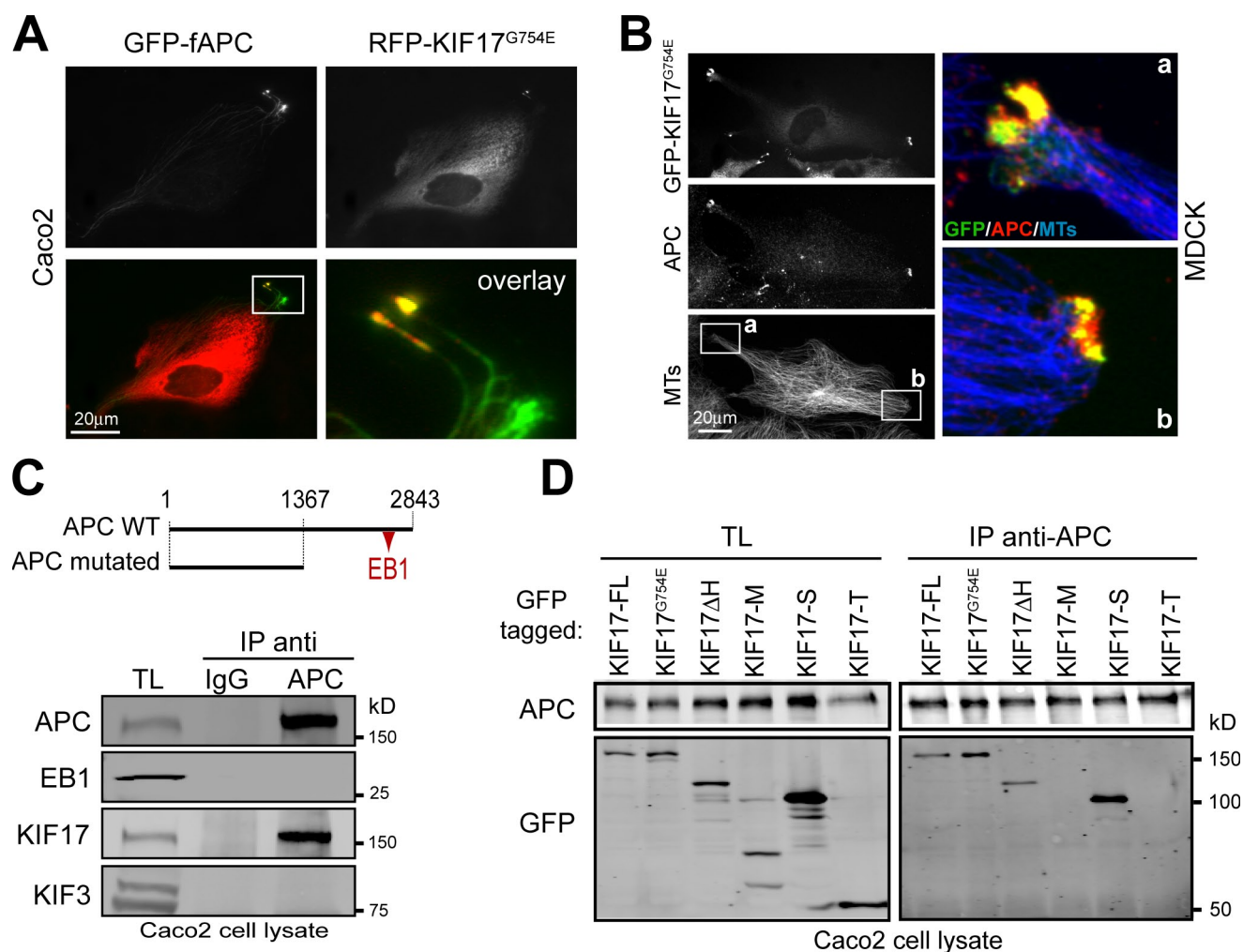
Figure 5. **KIF17 coiled-coil region binds APC independently of EB1.** (A) Colocalization of GFP-fAPC and mRFP-KIF17^G754E at plus ends of a subset of MTs in Caco2 cells 3 h after cDNA injection. The boxed region is magnified on the right. (B) Immunostaining of APC and tyrosinated tubulin in MDCK cells expressing GFP-KIF17^G754E. Color overlays (a and b) show magnifications of the boxed regions. (C) Schematic of wild-type (WT) and C-terminally truncated APC present in Caco2 cells. The red arrowhead shows the EB1 binding site, which is missing in Caco2 APC. Immunoblots show endogenous APC, EB1, KIF17, and KIF3 in total lysates (TL) and immunoprecipitates from Caco2 cells incubated with rabbit IgG or anti-APC IgG. Numbers on top indicate amino acid position. (D) Immunoblots showing total lysates and immunoprecipitated APC (endogenous) and GFP-KIF17 constructs expressed in Caco2 cells.

KIF17 interacts with APC and colocalizes with APC at the plus ends of a subset of MTs

APC hitchhikes on EB1, but recent work suggests this may not be the only mechanism by which it associates with MT ends (Jimbo et al., 2002; Kita et al., 2006; Sharma et al., 2006). Like KIF17, APC accumulates at the plus ends of a subset of MTs (Näthke et al., 1996). When coexpressed in MDCK (not depicted) or Caco2 cells, full-length APC (GFP-f-APC) and mRFP-KIF17^G754E colocalize at the ends of the same subset of MTs (Fig. 5 A). In addition, GFP-KIF17^G754E and endogenous APC in MDCK cells colocalize at MT tips in cell extensions (Fig. 5 B). Given this colocalization, we tested if KIF17 could interact with APC independently of EB1. APC in Caco2 cells is truncated at aa 1367 and thus does not interact with EB1 (Fig. 5 C; Askham et al., 2000; Rowan et al., 2000). Incubation of Caco2 lysates with APC antibodies resulted in coprecipitation of KIF17 with APC, but as expected, not EB1 (Fig. 5 C). KIF3 did not coprecipitate with APC under these conditions

(Fig. 5 C). Immunoprecipitation of endogenous APC from Caco2 cells expressing various GFP-tagged KIF17 constructs shows that APC interacts with KIF17 through its stalk domain (Fig. 5 D). Both KIF17^G754E and KIF17ΔH (deletion of the hinge, aa 463–738) also interacted with APC, demonstrating that the interaction is mediated by KIF17 coiled-coil regions (Fig. 5 D). Thus, the N-terminal region of APC binds the stalk domain of KIF17 independently of EB1.

KIF17 is necessary for APC localization at MT ends in cell protrusions

We next analyzed the effect of overexpressed GFP-KIF17-S on localization of endogenous APC in MDCK cells. In un-injected controls, APC localized at the tip of MTs, converging in cell extensions in 83% of cells. In contrast, only 21% of cells expressing KIF17-S had APC at MT tips in cell extensions (Fig. 6, A and B). Localization of APC at these sites was also decreased in cells expressing GFP-KIF17^G754E-G243A and KIF17^G754E-R288/294A, which do not associate with MT plus

ends, suggesting that KIF17 motor activity is required for this function (Fig. S2). KIF17 depletion resulted in clear reduction of endogenous APC from MT plus ends in cell extensions as compared with controls (Fig. 6 C). The localization of APC at MT plus ends could be rescued by rapid and acute expression (injection of cDNA) of KIF17^{G754E} (Fig. 6 D). Together, these data show that KIF17 is necessary but not sufficient for APC localization at the ends of MTs converging in cell extensions.

KIF17 affects the level of acetylated MTs

EB1 and APC are key players in regulation of MT dynamics and stabilization in fibroblasts (Fukata et al., 2001, 2002; Watanabe et al., 2004; Wen et al., 2004; Kroboth et al., 2007). Because KIF17 interacts with EB1 and APC, we hypothesized that KIF17 could influence MT arrays in epithelial cells. We infected MDCK cells with control or KIF17 small hairpin RNA (shRNA) and immunostained tyrosinated tubulin (labels dynamic MTs) and acetylated tubulin (a marker of stabilized MTs; Piperno et al., 1987). KIF17 knockdown did not alter tyrosinated MT arrays but reduced the amount of acetylated MTs detected by immunofluorescence as compared with controls (Fig. 7 A). In immunoblots, we measured a 57% decrease in acetylated tubulin in KIF17-depleted cells (Fig. 7 C). Similar results were obtained with Caco2 cells (Fig. S4). In both cell types, the decrease in acetylated tubulin levels was proportional to the amount of KIF17 depleted from cells. Conversely, overexpression of GFP-KIF17^{G754E}, but not GFP-KIF17$^{G754E-G243A}$ or KIF17$^{G754E-R288/294A}$, increased the amount of acetylated MTs detected by immunofluorescence (Figs. 7 B and S3 A) and acetylated tubulin detected by Western blotting (Fig. 7 C). In addition, injection of GFP-KIF17^{G754E} cDNA in KIF17-depleted cells restored acetylated MT staining to normal levels (Fig. 7 D). These results indicate that active, MT-associated KIF17 contributes to the generation of acetylated MTs in epithelia. This likely reflects a role for KIF17 in MT stabilization (see the following sections), as acetylation is a modification associated with stabilized MTs.

KIF17 alters MT dynamicity and decreases MT polymerization rates

We next analyzed the effects of KIF17 overexpression and knockdown on MT dynamics in Caco2 cells expressing EB1-GFP. MT dynamics were measured by tracking the net displacement of EB1-FL-GFP at MT plus ends in sequential frames of time-lapse images (Fig. 8 A; Salaycik et al., 2005). We observed two types of EB1-GFP displacements: persistent or nonpersistent growth. In control cells (shNC or RFP), 48% of EB1-labeled MTs grew persistently during a 20-s period (Fig. 8 B). The remaining 52% underwent catastrophe, rescue, or pause (imaging MT dynamics with EB1 cannot distinguish between these parameters of dynamicity). In cells expressing KIF17 shRNA (30% depletion) or mRFP-KIF17-FL^{G754E}, persistent MT growth decreased by 20% and 44%, respectively, whereas the number of EB1-labeled MTs undergoing catastrophe, rescue, or pause increased proportionately (Fig. 8 B). Persistently growing, EB1-labeled MTs polymerized with an average rate
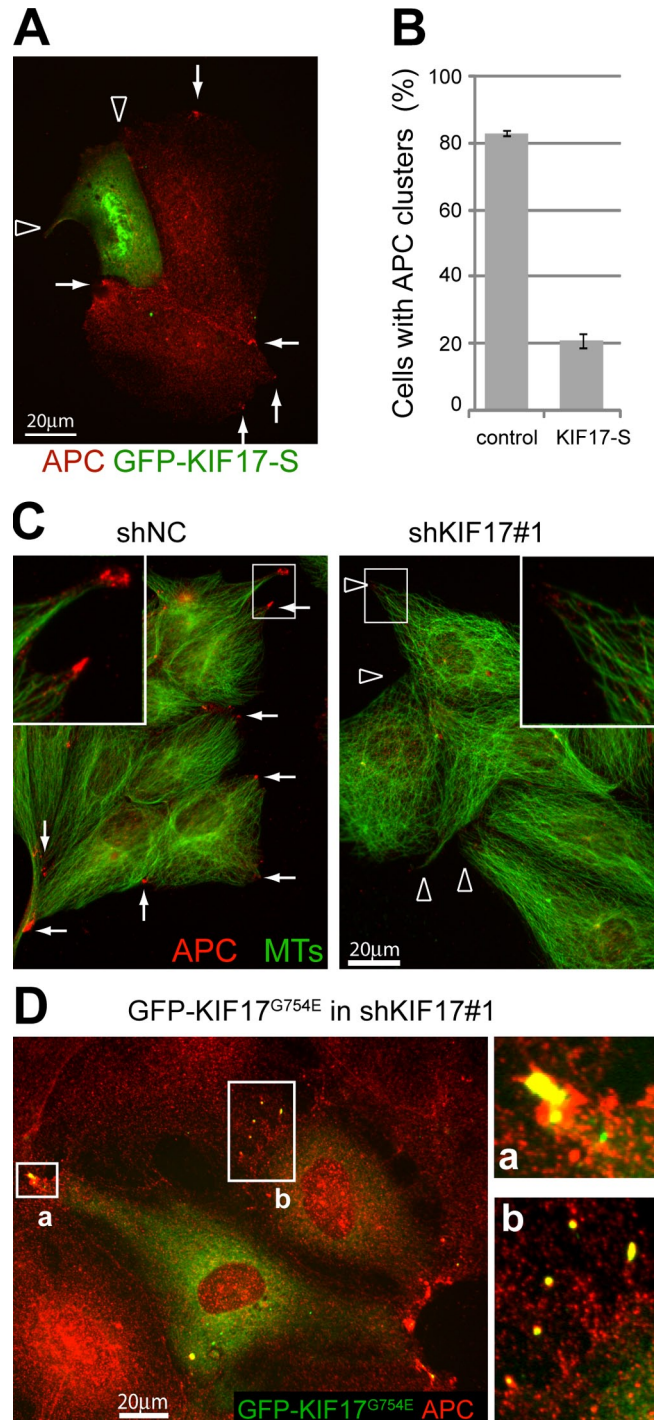

Figure 6. **KIF17 is necessary for APC localization at MT plus ends.** (A) Immunostaining of endogenous APC (red) in MDCK cells fixed 1 d after transfection with GFP-KIF17-S (green). Arrows, APC clusters in cell protrusions in nonexpressing cells; arrowheads, protrusions lacking APC in a cell expressing GFP-KIF17-S. (B) Percentage of GFP-KIF17-S–expressing cells (n = 183) or surrounding controls (n = 189) with APC clusters in protrusions. Data were compiled from three experiments. Error bars indicate SEM. (C) Immunostaining of APC and MTs in MDCK cells expressing control (shNC) or KIF17 (shKIF17#1) shRNAs. Arrows, APC clusters localizing at MT ends in cell protrusions; arrowheads, cell protrusions lacking APC clusters at MT ends. Insets show enlarged views of the boxed regions. (D) Rescue of APC localization in cell protrusions by expression of GFP-KIF17^{G754E} in KIF17-depleted MDCK cells. Boxed regions are shown at high magnification on the right.
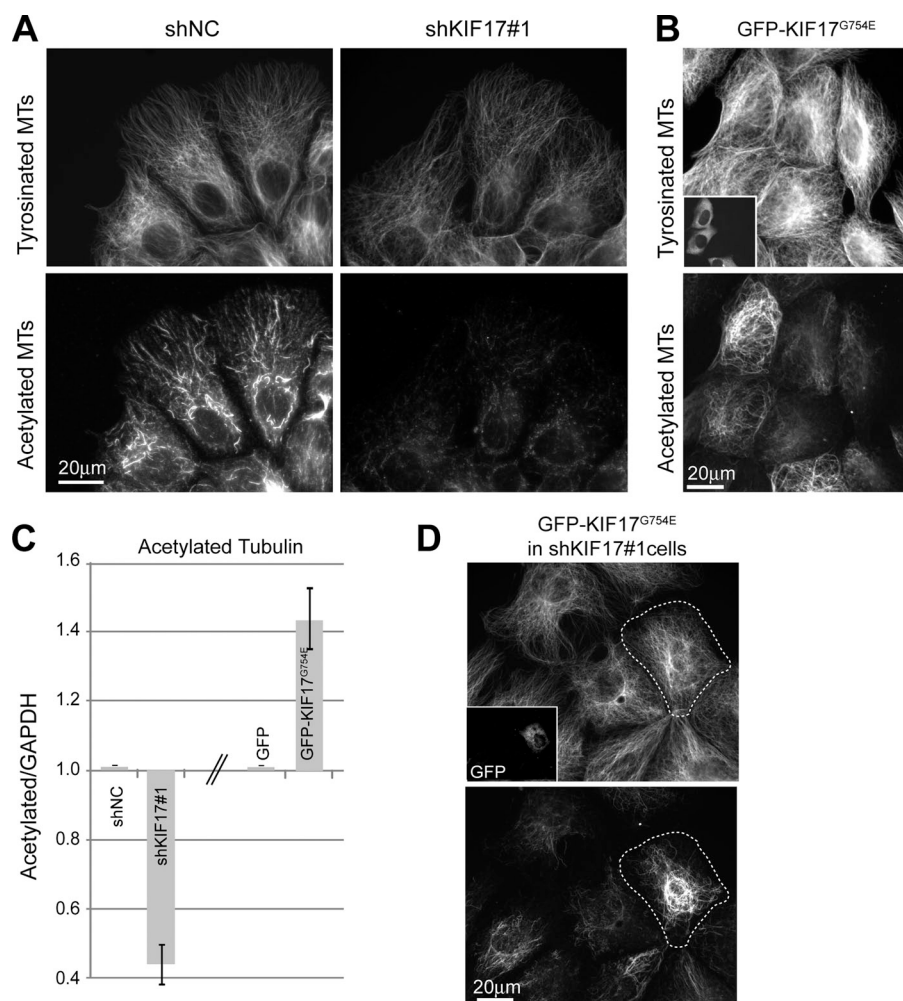
A shNC shKIF17#1

Tyrosinated MTs

Acetylated MTs

20μm

B GFP-KIF17^{G754E}

Tyrosinated MTs

Acetylated MTs

20μm

Figure 7. **KIF17 affects MT acetylation in epithelial cells.** (A and B) Immunostaining of tyrosinated and acetylated tubulin in MDCK cells infected with control (shNC) or KIF17 (shKIF17#1) shRNA (A), or fixed 5 h after microinjection of GFP-KIF17^{G754E} cDNA (B). (C) Quantitative immunoblot analysis of acetylated tubulin in MDCK cells treated with control or KIF17 shRNA, or expressing GFP or GFP-KIF17^{G754E}. The ratio of acetylated tubulin/GAPDH was normalized to 1 in controls. Data were derived from 3–5 experiments. Error bars indicate SEM. (D) KIF17-depleted MDCK cells fixed 3 h after injection of GFP-KIF17^{G754E} cDNA and stained for tyrosinated and acetylated MTs. Outlined regions indicate injected cells. Insets show the injected GFP-KIF17^{G754E}.

C Acetylated Tubulin

Acetylated/GAPDH (y-axis: 0.4, 0.6, 0.8, 1.0, 1.2, 1.4, 1.6)

shNC, shKIF17#1, GFP, GFP-KIF17^{G754E}

D GFP-KIF17^{G754E} in shKIF17#1 cells

GFP

20μm

of 11.51 µm/min and 10.97 µm/min, respectively, in shNC or RFP controls. In KIF17-depleted cells, MTs grew 30% faster, with an average rate of 15 µm/min (Fig. 8, B and C). Conversely, expression of mRFP-KIF17-FL^{G754E} reduced the mean MT polymerization rate by 25% to 8.28 µm/min (Fig. 8, B and D). In addition, MT polymerization measured in cells expressing EB1-FL^{EE}-GFP, which exhibits reduced KIF17 binding (Fig. 3 E), was 11% faster (12.8 µm/min) than those measured in cells expressing EB1-FL-GFP (11.6 µm/min, Fig. 8 E). C-terminal fusions of GFP to EB1 have been found to alter its binding to other proteins, and may modify its activity at MT tips (Skube et al., 2010), so we also analyzed the behavior of GFP-EB1, and obtained similar results (GFP-EB1-FL, 12 µm/min; GFP-EB1-FL^{EE}, 15.1 µm/min; GFP-EB1-FL in shNC, 11.44 µm/min; GFP-EB1-FL in shKIF17, 12.73 µm/min). These data show that KIF17 is involved in regulating MT polymerization rates and dynamics in epithelial cells.

KIF17 promotes MT plus end stabilization

MTs can be stabilized by a plus end capping mechanism that prevents addition or loss of tubulin subunits. These stabilized MTs are resistant to depolymerization by MT antagonists. To determine if the effects of KIF17 overexpression or depletion on acetylated MTs reflect changes in MT stability, we treated

MDCK cells with 33 µM NZ. In cells expressing control shRNA, tyrosinated, dynamic MTs depolymerized completely after 1 h in NZ, whereas a population of acetylated MTs persisted. In cells expressing KIF17 shRNA, the number of NZ-resistant, acetylated MTs diminished significantly (Fig. 9 A). Conversely, in cells expressing GFP-KIF17^{G754E}, but not GFP-KIF17$^{G754E-G243A}$ or KIF17$^{G754E-R288/294A}$, a robust array of acetylated MTs persisted after NZ treatment as compared with neighboring, noninjected controls (Fig. 9 B and S3 B). Time-lapse imaging demonstrated directly that MTs labeled with GFP-KIF17^{G754E} are resistant to NZ-induced MT depolymerization (Fig. 9 C, video not shown). This suggests that KIF17 may function as part of the MT plus end capping machinery to stabilize MTs.

KIF17 contributes to epithelial polarization

MT reorganization and stabilization is a prominent event associated with epithelial polarization. Furthermore, MTs are essential for polarization of apical membrane proteins, as they support trafficking to this membrane (Rindler et al., 1987; Eilers et al., 1989; Matter et al., 1990; Gilbert et al., 1991; Saunders and Limbird, 1997). In 3D cultures, apical polarization occurs at the 2–4-cell stage of cystogenesis through a process that includes transcytosis of apical markers from the basal membrane (cyst periphery) to a preapical patch localized at the internal face of cysts
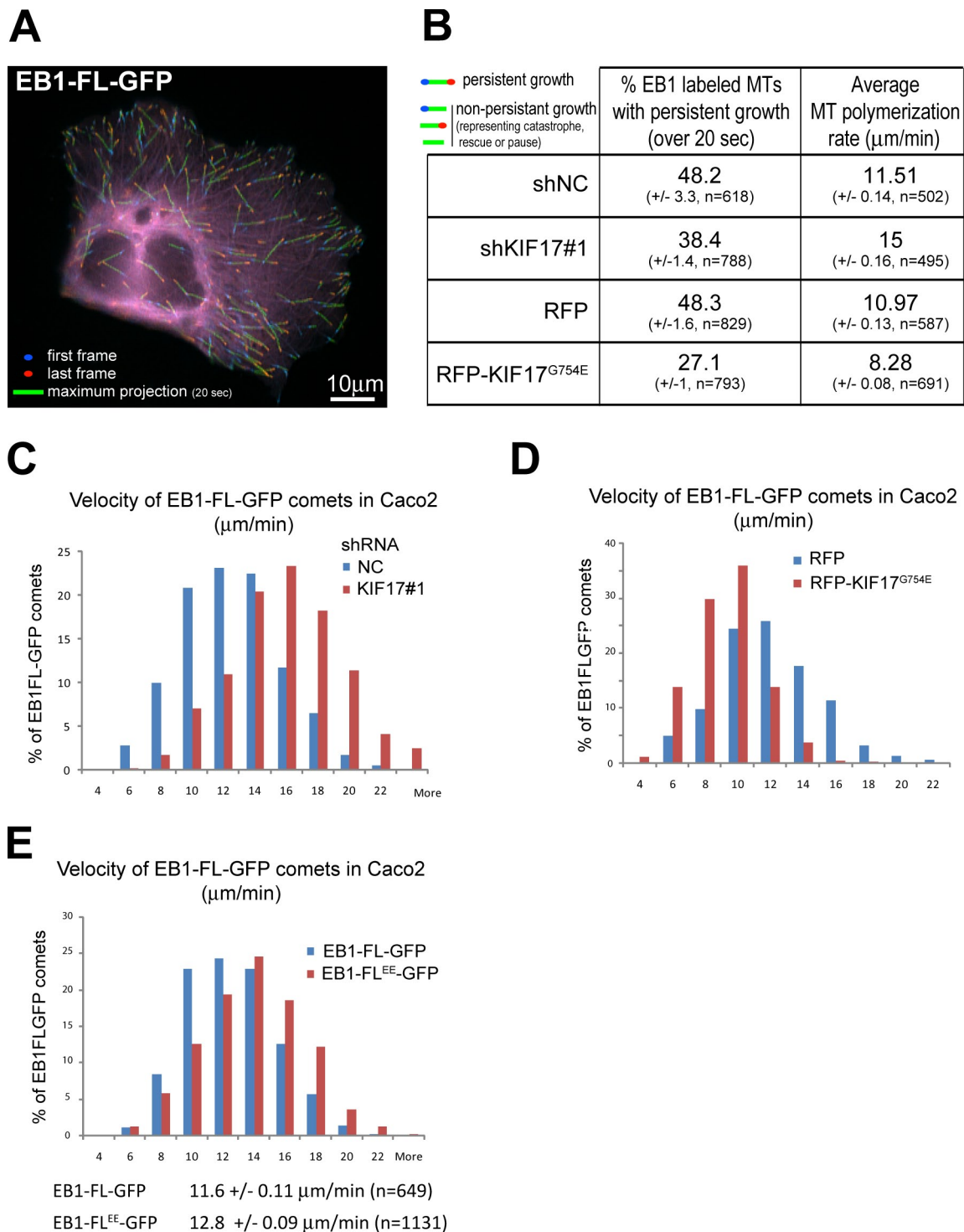
A

EB1-FL-GFP

• first frame
• last frame
— maximum projection (20 sec)

10μm

B

●—● persistent growth

●—● non-persistent growth (representing catastrophe, rescue or pause)

	% EB1 labeled MTs with persistent growth (over 20 sec)	Average MT polymerization rate (μm/min)
shNC	48.2 (+/- 3.3, n=618)	11.51 (+/- 0.14, n=502)
shKIF17#1	38.4 (+/-1.4, n=788)	15 (+/- 0.16, n=495)
RFP	48.3 (+/-1.6, n=829)	10.97 (+/- 0.13, n=587)
RFP-KIF17^{G754E}	27.1 (+/-1, n=793)	8.28 (+/- 0.08, n=691)

C

Velocity of EB1-FL-GFP comets in Caco2 (μm/min)

shRNA
■ NC
■ KIF17#1

D

Velocity of EB1-FL-GFP comets in Caco2 (μm/min)

■ RFP
■ RFP-KIF17^{G754E}

E

Velocity of EB1-FL-GFP comets in Caco2 (μm/min)

■ EB1-FL-GFP
■ EB1-FL^{EE}-GFP

EB1-FL-GFP   11.6 +/- 0.11 μm/min (n=649)

EB1-FL^{EE}-GFP   12.8 +/- 0.09 μm/min (n=1131)

Figure 8.   **KIF17 attenuates MT polymerization.** (A) Maximum projection of EB1-FL-GFP in 10 sequential frames (2-s intervals) of a time-lapse recording of Caco2 cells. EB1-GFP was expressed by cDNA microinjection. The first frame is shown in blue, the last frame in red, and intermediary frames in green. (B) Analysis of EB1-GFP–labeled MT dynamics (persistent growth) and mean polymerization rates (net displacement/time) in Caco2 cells expressing control (shNC) or KIF17 (shKIF17#1) shRNAs and in cells expressing RFP or RFP-KIF17^{G754E}. Data compiled from at least five cells/experiment in three experiments. n = the number of EB1-labeled MTs analyzed. (C–E) Histograms show polymerization rates of EB1-GFP–labeled MTs in Caco2 cells infected with shNC or shKIF17#1 (C), coexpressing RFP or RFP-KIF17^{G754E} (D), or expressing EB1-FL-GFP or EB1-FL^{EE}-GFP (E). Data were compiled from at least six cells per experiment in three experiments. n = the number of EB1-labeled MT ends analyzed.

(Meder et al., 2005; Ferrari et al., 2008). We infected subconfluent MDCK cells with control or KIF17 shRNAs. Cells were reseeded as single cells in Matrigel 6 d later, when KIF17 levels were reduced by ~60%. In 83% of cells expressing control shRNA, the early apical marker GP135 was excluded from the periphery of 2–4-cell cysts and had transcytosed to either a preapical patch or the apical membrane facing the lumen as described previously (Fig. 10, A, inset, and B; Meder et al., 2005; Ferrari et al., 2008).
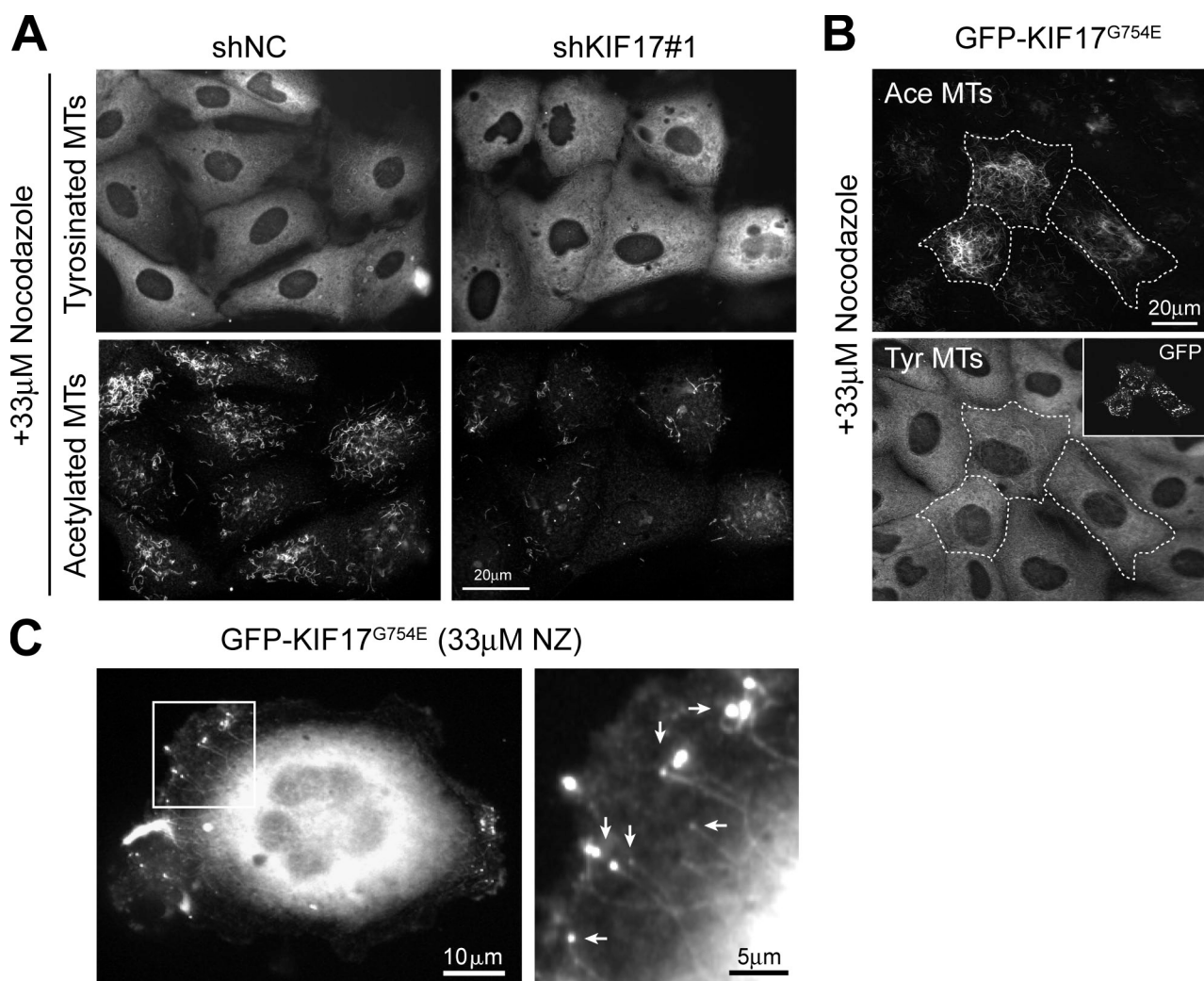
Figure 9. KIF17 affects MT stabilization in epithelial cells. (A) Immunostaining of tyrosinated and acetylated tubulin in MDCK cells infected with shNC or shKIF17#1 and treated for 45 min with 33 µM NZ. (B) Acetylated and tyrosinated tubulin in MDCK cells (outlined cells and inset), treated for 1 h with 33 µM NZ. (C) Caco2 cells injected with GFP-KIF17^{G754E} cDNA and treated for 15 min with 33 µM NZ. An enlargement of the boxed region is shown on the right. Arrows point to GFP-KIF17^{G754E} at the ends of NZ-resistant MTs.

In contrast, GP135 localized at the cyst periphery or had a non-polarized distribution in 52% and 18%, respectively, of cysts grown from KIF17-depleted cells (Fig. 10, A and B). This suggests that KIF17 has a role in polarization of apical markers during early cystogenesis.

After 5 d in culture, 90% of controls formed cysts comprised of a cell monolayer surrounding a single central lumen (Fig. 10, C and D). In contrast, KIF17 depletion decreased the number of cysts with a single lumen to 57%, with a corresponding increase in cysts with multiple lumens (35%) or no lumen (7%; Fig. 10 D). Immunostaining revealed that GP114 localized apically in 93% of control cysts but showed a nonpolar distribution in 47% of KIF17-depleted cysts (Fig. 10, C and E). Similar results were observed in Caco2 cells, where KIF17 depletion inhibited the apical accumulation of atypical PKC (Fig. S4). Together, our results suggest that KIF17 contributes to epithelial morphogenesis and apical polarity by modifying formation of stable MT arrays. In support of this idea, we found that acetylated MTs are concentrated at the apical pole of cells in MDCK cysts (Fig. 10 F).

Discussion

In mammalian cells, KIF17 transports vesicles containing *N*-methyl-D-aspartate receptor and K$^+$ channel subunits to dendrites (Setou et al., 2000; Chu et al., 2006). KIF17 also transports KV1.5 in cardiac myocytes (Cai et al., 2009) and a cyclic nucleotide gated channel subunit to primary cilia in epithelia (Jenkins et al., 2006). In *C. elegans* and *Danio rerio*, KIF17 homologues play critical roles in ciliogenesis and intraflagellar particle transport in neuronal sensory cilia and in photoreceptors (Snow et al., 2004; Insinna et al., 2008). We also found that in polarized epithelia, KIF17 could be detected in primary cilia (unpublished data).

Here, we show that KIF17 associates with MT plus ends, where it contributes to regulation of MT dynamics, polymerization rates, and MT plus end stabilization. KIF17 targeting to MT plus ends requires ATPase activity and interaction with EB1. KIF17 also interacts with APC and regulates its localization on a subset of MT ends converging in cell extensions. We also found
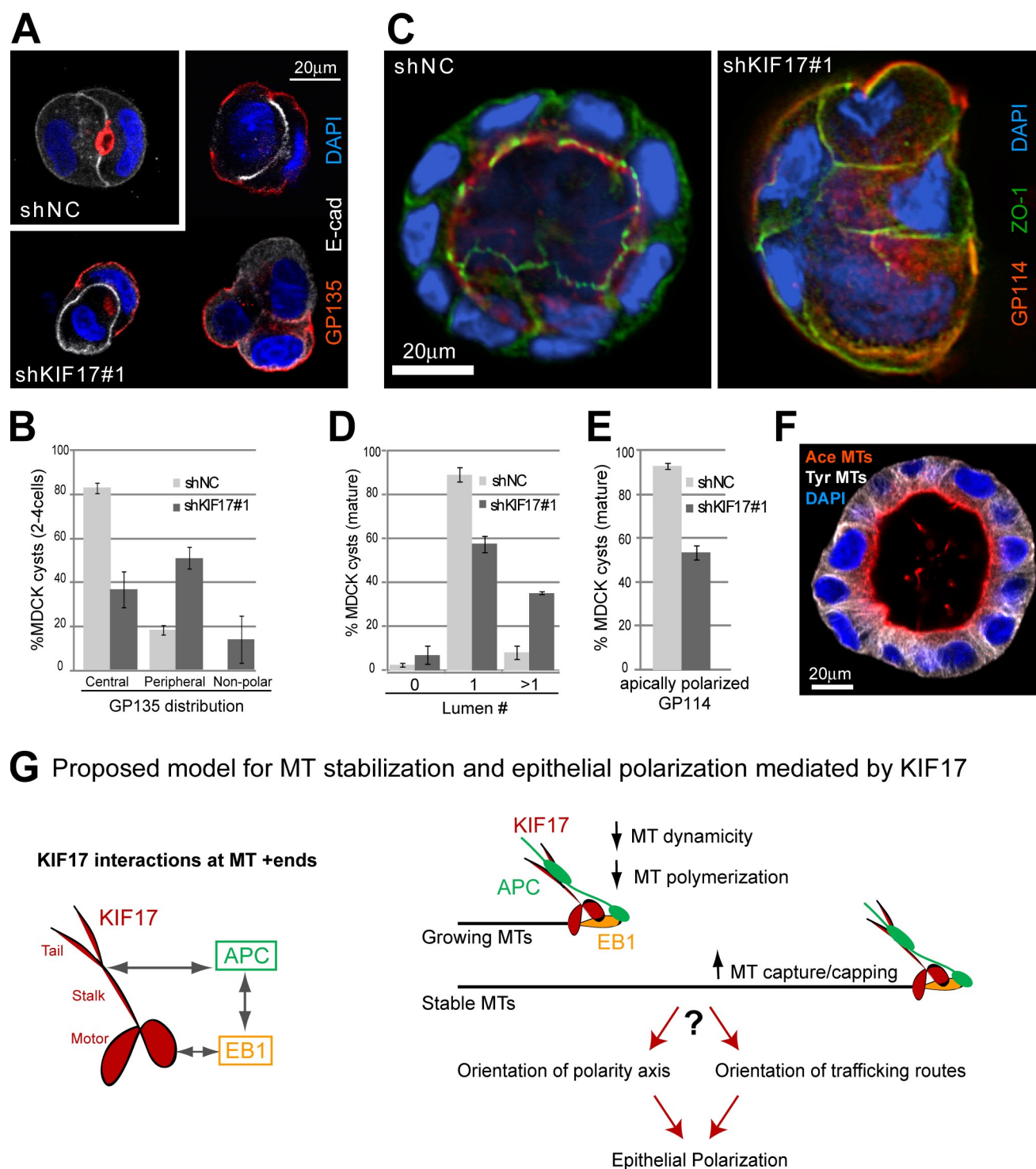
G Proposed model for MT stabilization and epithelial polarization mediated by KIF17

Figure 10. **KIF17 participates in epithelial cystogenesis.** (A) Immunolocalization of GP135, E-cadherin, and DAPI in control (shNC) and KIF17-depleted (shKIF17#1) MDCK cysts grown 2 d in Matrigel. (B) Quantification of 2–4 cell cysts with central, peripheral, and nonpolarized GP135 localization. (C) Immunolocalization of GP114, ZO-1, and DAPI in control and KIF17-depleted MDCK cysts grown 5 d in Matrigel. (D) Graph shows percentage of cysts with 0, 1, or >1 lumen. (E) Percentage of cysts with apically polarized GP114. All analyses are derived from three independent experiments; 100–200 cysts were analyzed per condition. (F) Tyrosinated tubulin, acetylated tubulin, and DAPI staining in mature control cyst. Error bars indicate SEM. (G) Proposed role for KIF17 in MT stabilization and epithelial polarization.

KIF17 has a role in apico-basolateral polarization and formation of a single, central lumen during epithelial cystogenesis. We propose that KIF17, via targeting by EB1, exerts a net transport necessary for MT plus end tracking of APC and perhaps other +TIPs to stabilize MTs in epithelial cells. KIF17 effects on MT stability may define a polarity axis that orients intracellular membrane trafficking, leading to apico-basolateral polarization and normal morphogenesis. To our knowledge, this is the first demonstration

of an anterograde kinesin contributing to localization of known +TIPs and MT stabilization in metazoa, and it highlights the importance of MT stabilization in 3D polarization of epithelial cells.

Targeting KIF17 to MT plus ends

Several proteins track MT plus ends and regulate MT dynamics by interacting with the C-terminal coiled-coil region of EB1 (Akhmanova and Steinmetz, 2008). The anterograde kinesin Tea2, in *S. pombe*, interacts with Mal3 (EB1) via its short N-terminal extension (Browning and Hackney, 2005). A weak interaction between Mal3 and the Tea2 motor domain was also reported. KIF17 does not contain an N-terminal extension and its binding to EB1 is instead mediated by its motor domain. This suggests that EB1 targets KIF17 to MT ends by regulating its ATPase activity or its binding to/retention at MT plus ends. In time-lapse recordings, we observed both GFP-KIF17-FL and mutant GFP-KIF17^{G754E} moving along linear paths toward MT plus ends and some KIF17 puncta that remained transiently at MT ends. This is consistent with results showing that a KIF17 mutant (aa 1–490) dwells at MT plus ends labeled by EB3 (Cai et al., 2009). Interestingly, a recent study showed Ca^{2+}-dependent binding of the kinesin-1 motor domain with the Rho-GTPase Miro (Wang and Schwarz, 2009). This Ca^{2+}-stimulated binding inhibits the interaction of kinesin-1 with MTs and its transport of mitochondria in neurons. Together, these results support a model of kinesin regulation wherein protein–protein interactions via the kinesin motor domain influence MT binding.

Although interaction of the KIF17 motor domain with EB1 is necessary for its MT plus-end targeting, it is not sufficient; kinesin MT binding and ATPase activities are also required. In addition, overexpressed KIF17 motor domain does not accumulate at MT plus ends (unpublished data), which suggests that KIF17 requires another factor, likely interacting with the stalk and/or tail domain, to associate with MT plus ends. This is consistent with MT tip tracking behavior of Tea2 in *S. pombe*, which requires both Mal3 and its cargo, Tip1 (Browning et al., 2003; Bieling et al., 2007). Thus, we propose that targeting and activation of KIF17 involves a dual regulatory mechanism wherein interaction of the kinesin head with EB1 and the stalk/tail with cargo regulates the ability of this motor to interact preferentially with MT plus ends.

Interestingly, KIF17 appears as discrete puncta at MT ends instead of comet-like structures characteristic of treadmilling proteins. This is similar to what was described for yeast Tea2 and Kip2, and their cargo, most likely because they accumulate at MT plus ends by net transport (Browning et al., 2000; Browning et al., 2003; Carvalho et al., 2004). APC also localizes as puncta rather than comets at MT ends (Mimori-Kiyosue et al., 2000a), which suggests it may indeed be a bona fide cargo of KIF17.

Kinesin-mediated transport at MT plus ends

In fungi, anterograde kinesins are needed for MT plus end transport of cargo that control MT dynamics, cortical capture, and polarized cell growth. In metazoa, homologues of these cargo have only been described to tip track by hitchhiking or treadmilling mechanisms (Wu et al., 2006). This has led to speculation that kinesin-mediated transport at MT tips was lost during evolution. Our findings suggest this is not the case. Localization of APC at MT ends is dependent on its interaction with KIF17, which suggests it is a cargo of KIF17 in epithelial cells. Although APC can interact with KIF17 independently of EB1, this is not sufficient for association with MT ends, as truncated APC found in Caco2 cells, which lacks an EB1 binding domain (Askham et al., 2000; Rowan et al., 2000), does not localize to MT plus ends. This is consistent with previous studies showing that interaction between the C-terminal region of APC and EB1 is required for APC MT tip tracking (Mimori-Kiyosue et al., 2000a). Thus, localization of APC to MT ends likely relies on formation of a tripartite complex with EB1 and KIF17. APC was shown to interact with KAP3, the nonmotor accessory protein of the kinesin-2 family member KIF3A/B (Jimbo et al., 2002). This interaction is presumed to mediate APC transport on MTs. However, in our hands, KIF3 did not localize to MT plus ends or interact with EB1 or APC. In *C. elegans*, KIF3 and KIF17 homologues cooperate to transport IFT particles along proximal and distal segments, respectively, of neuronal sensory cilia (Snow et al., 2004). Thus, it is possible that APC transport along MTs could be mediated by KIF3, whereas its association with MT plus ends may depend on KIF17.

Asymmetric accumulation of APC at the ends of a subset of MTs oriented along the long axis of cells is unique among MT tip tracking proteins, and its significance is still unclear (Näthke et al., 1996). KIF17 has a similar asymmetric distribution and colocalizes with APC on the same MT plus ends. Quantitative analysis of endogenous KIF17 revealed that it co-localizes with approximately half of EB1-labeled MTs at random regions in cells but is enriched approximately twofold on MTs converging in cell extensions. KIF17^{G754E} exhibits a more dramatic asymmetric distribution and is detected primarily at the ends of this subset of MTs. We believe that KIF17^{G754E}, like endogenous KIF17, associates with plus ends of more MTs in the cytoplasm, but that it is difficult to detect unambiguously at these sites. Supporting this, we found that KIF17^{G754E} alters the dynamics and polymerization rates of MTs located in all areas of the cytoplasm. Thus, KIF17 is a second MT plus end–associated protein that exhibits an asymmetric distribution at the ends of a subset of MTs. This could occur if KIF17 recognizes a population of MTs with distinct properties, such as posttranslationally modified tubulin subunits. Selective interactions with subsets of modified MTs were described for KIF5 and KIF1A (Liao and Gundersen, 1998; Reed et al., 2006; Ikegami et al., 2007; Dunn et al., 2008; Konishi and Setou, 2009). However, a recent study suggests that KIF17 does not exhibit a preference for modified or unmodified MTs (Cai et al., 2009). Alternatively, signaling from localized, cortical factors that can act on the cargo or kinesin might influence the distribution of KIF17 to subsets of MT ends in cells.

Regulation of MT stabilization by KIF17

Using cellular and biochemical approaches, we showed that KIF17 has a positive role in MT stabilization in epithelia. KIF17 also attenuates polymerization rates and dynamics in

EB1-labeled MTs, which suggests that it regulates parameters of MT dynamic instability like Tea2. However, Tea2 acts as an inhibitor of MT catastrophe by transporting the anticatastrophe factor Tip1 (CLIP170) to MT plus ends (Busch et al., 2004). Whether KIF17 modifies MT polymerization rates directly or indirectly, by transporting cargo that regulates MT dynamics or stabilization, is still unclear. However, APC was shown to stabilize MTs in PTK2 epithelial cells and in vitro (Zumbrunn et al., 2001). Attenuation of MT polymerization rates and APC targeting by KIF17 could be envisioned to favor an interaction between MT ends and cortical proteins involved in MT capture and stabilization.

MT stabilization can be mediated by a plus end capping mechanism that prevents addition and loss of tubulin subunits from MT plus ends (Webster et al., 1987; Khawaja et al., 1988; Webster and Borisy, 1989). Altered resistance of MTs to NZ in cells depleted of or overexpressing KIF17 suggests that KIF17 contributes to MT capping. Although components of a MT plus-end cap are not known, capping in TC-7 epithelial cells involves an ATPase activity with characteristics of kinesin (Infante et al., 2000). Consistent with this, ATPase-deficient KIF17$^{G754E-G243A}$, which binds MTs but does not accumulate at plus ends, does not enhance MT stability or acetylation. This suggests that KIF17 activity at MT ends contributes to MT stabilization and that KIF17 could be involved in MT plus end capping. Indeed, time-lapse imaging of MTs decorated by GFP-KIF17^{G754E} shows these MTs are resistant to NZ and that KIF17^{G754E} remains on the ends of these MTs during drug treatment. Together, our data support a model wherein KIF17 could promote formation of a complex between MT plus ends, via +TIPs such as APC, and cortical proteins to capture and selectively cap MTs in epithelial cells. This is significant as it provides the first evidence in metazoa that an anterograde kinesin regulates MT stabilization.

Regulation of epithelial morphogenesis by KIF17

Generation of stable MT arrays is known to accompany epithelial polarization. Whether MT stabilization is a trigger for or a consequence of this polarization is still debated. In neurons, localized stabilization of MTs is sufficient for axon specification (Witte et al., 2008), demonstrating that MT stabilization can precede polarization. Similarly, we find KIF17 positively effects MT stabilization in epithelia and is necessary for polarization of cells in 3D matrices. Depletion of KIF17 results in slow-growing, disorganized cysts that often lack a lumen or contain multiple lumens. These cells also often failed to polarize apical markers. Mechanistically, KIF17 could contribute to polarization through its established role in membrane trafficking (Setou et al., 2000; Guillaud et al., 2003; Chu et al., 2006; Jenkins et al., 2006; Cai et al., 2009). Alternatively, KIF17 could contribute to polarization by a mechanism involving selective MT stabilization and establishment of polarized trafficking routes to the apical pole. In support of this, we found that acetylated MTs are enriched in the apical cortex of cells grown in 3D matrices. These MTs could provide biochemically distinguishable tracks for other motors to transport vesicles toward the apical pole. For example, we reported that KIF5B mediates the transport of the

p75 neurotrophin receptor to the apical membrane of epithelial cells (Jaulin et al., 2007), and KIF5B interacts preferentially with detyrosinated and acetylated MTs (Liao and Gundersen, 1998; Reed et al., 2006). Alternatively, KIF17 could contribute to polarization in a manner similar to Tea2 and Kip2 in yeast by targeted transport of factors that regulate localized actin re-modeling at sites of polarized cell growth (Huyett et al., 1998; Browning et al., 2000; Konzack et al., 2005). Further studies are needed to resolve the mechanism through which KIF17 contributes to apico-basolateral membrane polarization and epithelial morphogenesis. However, our results provide novel insight into upstream effectors and downstream consequences of KIF17-mediated MT stabilization in epithelial cells.

Materials and methods

Cell culture, transfection, and microinjection
MDCK and HEK293 cells were cultured in DME (4.5 g/liter glucose) with 10% FBS and 20 mM Hepes, pH 7.2. Caco2 cells were cultured in DME with 10% FBS, 0.4 mM L-glutamine, 0.89 mM NaHCO$_3$, and nonessential amino acids. MDCK cells were seeded on sterilized coverslips and used at ~80% confluence 2–3 d after plating. Caco2 cells were seeded onto collagen-coated coverslips (rat tail type II; Sigma-Aldrich). For 3D cultures, cells were layered on Matrigel (BD) at 7 × 10^3 cells/well in 8-well chamber slides (Lab-Tek) in normal medium supplemented with 2% Matrigel as described previously (O'Brien et al., 2006). Cysts were fixed after 2 or 5 d in culture in 4% PFA for 30 min and permeabilized with 0.5% Triton X-100 for 15 min. Transfections (5 µg DNA or 0.5–3 µg siRNA) were performed using Lipofectamine 2000 (Invitrogen) for HEK293 cells or the Amaxa nucleofector (Amaxa Inc., Gaithersburg, MD) for MDCK and Caco2 cells as recommended. Microinjection was performed essentially as described previously (Jaulin et al., 2007). cDNAs (5–20 µg/ml) in HKCl (10 mM Hepes and 140 mM KCl, pH 7.4) were injected using a micromanipulator (Narishige). Cells were incubated at 37°C for 60–90 min to allow for expression of cDNAs.

Expression constructs
KIF17 and EB1 were amplified by PCR from human A549 or Caco2 cells and cloned into Gateway expression vectors (Invitrogen). Primers used were as follows. KIF17-FL (aa 1–1029): forward, 5'-ATGGCCTCCGAG-GCGGTGAA-3'; and reverse, 5'-TCACAGAGGCTCACTGCCAAAGTT-3'. KIF17-Motor (aa 1–339): forward, 5'-ATGGCCTCCGAGGCGGTGAA-3'; and reverse, 5'-TCAGCGCGGCTTGTTCCTGATGTT-3'. KIF17-M-Δ5 (aa 6–339): forward, 5'-ACAAGTTTGTACAAAAAAGCAGGCTTCGT-GAAGGTTGTCGTGCGCTGCCGTCCC-3'; and reverse, 5'-TGTTCAA-ACATGTTTTTTCGTCCGAAGCACTTCCAACAGCACGCGACGGCT-GGG-3'. KIF17-Stalk (aa 340–849): forward, 5'-ATCAATGAGGA-CCCCAAGGAT-3'; and reverse, 5'-TCACCGGCGGATGGTGGCCA-AGTA-3'. KIF17-Tail (aa 850–1029): forward, 5'-CAGGAGCGTGAC-TCCATGCTC-3'; and reverse, 5'-TCACAGAGGCTCACTGCCAAAGTT-3'. EB1-FL (aa 1–268): forward, 5'-GCAGTGAACGTATACTCAACG-3'; and reverse, 5'-TTAATACTCTTCTTGCTCCTCCTG-3'. EB1-N (aa 1–144): forward, 5'-GCAGTGAACGTATACTCAACG-3'; and reverse, 5'-TTATGGAG-CAACAAGGGAAGG-3'. EB1-C (aa 145–268): forward, 5'-GCTCT-GAATAAACCGAAGAAAC-3'; and reverse, 5'-TTAATACTCTTCTTGCT-CCTCCTG-3'. EB1Δ7 (aa 1–261): forward, 5'-GCAGTGAACGTATACT-CAACG-3'; and reverse, 5'-TTATGGGCCCCCCTTCATCAGG-3'. KIF3A-FL (1–702): forward, 5'-ATGCCGATCAATAAATCAGAGAAGCC-3'; and reverse, 5'-TTACTGCAGTAAAGAGTCAATTACAGT-3'. KIF5B-Motor (aa 1–335): forward, 5'-ATGGCGGACCTGGCCGAGTGC-3'; and reverse, 5'-AGTTAACTCCACATTGACACAAACTGTGTT-3'. Mutant KIF17-FL^{G754E}, KIF17-M^{IP}, and EB1-FL^{EE} were produced by site-directed mutagenesis using the QuickChange kit (Agilent Technologies). KIF17^{G754E}: forward, 5'-CTGCAGCTGTTGGAGCAGCAGGTTGTGGAAGGAGAGCAGGCC-AAGAAC-3'; and reverse, 5'-GTTCTTGGCCTGCTCTCCTTCCACAACCT-GCTGCTCCAACAGCTGCAG-3'. KIF17^{G243AE}: forward, 5'-GCAAG-CTGAACCTGGTGGACCTGGCGGCCAGCGAGCGGCAGTCCAAGA-CC-3'; and reverse, 5'-GGTCTTGGACTGCCGCTCGCTGGCCGCCAG-GTCCACCAGGTTCAGCTTGC-3'. KIF17$^{R288/294A}$: forward, 5'-CACGTC-CCCTACGCTGACTCGAAGCTGACGGCGCTGCTGCAGAC-3'; and

reverse, 5'-GTCCTGCAGCAGCGCCGTCAGCTTCGAGTCAGCGTA-GGGGACGTG-3'. KIF17-M[IP] (I[114]/P[115] to S[114]/S[115]): forward, 5'-CCGC-CCTCCCAGAGAGGCATCAGCTCCAGGGCCTTCGAGCACGTGTT-CGAG-3'; and reverse, 5'-GGCGGGAGGGTCTCTCCGTAGTCGAG-GTCCCGGAAGCTCGTGCACAAGCTC-3'. EB1-FL[EE] (E[211]/E[213] to A[211]/A[213]): forward, 5'-CTTACTGTTGAAGACTTGGCGAAAGCGAGGGA-TTTCTACTTCGGAAAGCTACGG-3'; and reverse, 5'-CTTTCCGAAG-TAGAAGTCTCTCGCCTTCGCCAAGTCTTCAACAGTAAG-3'. Mouse EB1-FL-GFP was provided by S. Tsukita (Kyoto University, Kyoto, Japan; Mimori-Kiyosue et al., 2000b). GFP-fAPC was provided by Y. Mimori-Kiyosue (KAN Institute, Inc., Kobe, Japan). EB1-C-GFP and EB1-C[EE]-GFP were provided by G. Gundersen (Columbia University, New York, NY; Wen et al., 2004).

Time-lapse and fixed cell imaging and analysis

After microinjection, cells were transferred to recording medium (Hanks balanced salt solution with 20 mM Hepes, 1% FBS, 4.5 g/liter glucose, and essential and nonessential amino acids with or without 100 µg/ml cycloheximide) and incubated at 37°C in a thermal-controlled chamber (Harvard Apparatus) on an epifluorescence microscope (TE-2000U; Nikon). Time-lapse and fixed cell images were acquired using a 60× Plan-Apochromat water immersion objective (NA 1.2) or 40× or 60× Plan-Apochromat oil immersion objective lenses (NA 1.0 or 1.4), respectively, and collected with a digital charge-coupled device camera (ORCA II-ER; Hamamatsu Photonics) at 1 MHz for 14-bit images. 14-bit images were scaled to illustrate features of interest as indicated in the Results and converted to 8-bit copies for figure assembly. All devices were controlled by MetaMorph software (Molecular Devices, Inc.), and postacquisition analysis and processing were performed with MetaMorph. Colocalization of KIF17 with EB1 or MT plus ends was measured using the Cell Scoring function after performing a background subtraction on each image. Background subtraction was performed using the mean pixel value of a noncell region on each image with the statistical correction function in MetaMorph. Random colocalization was measured after shifting the KIF17 image 10 pixels horizontally. Specific colocalization was calculated by subtracting random colocalization values for each image set. Velocity of EB1-FL-GFP comets on growing MTs was calculated based on net displacement over time during 1–2 min recordings. Only EB1 comets exhibiting plus-end directed movement in 10 or more sequential frames were analyzed. Maximum projections were assembled from images recorded at 2-s intervals. The distance between EB1-GFP in the first and last frames was used to calculate the rate of EB1-labeled MT polymerization. To minimize effects of EB1 overexpression on MT dynamics, 100 µg/ml cycloheximide was added 60 min after cDNA injection. Raw, 16-bit images were scaled using "scale image" so that the signal contributed by detector background noise was removed. High-intensity pixels in noncellular regions or regions not of interest were also scaled out. Images were then converted to 8-bit files for figure construction.

Images of 3D cysts were acquired with a scanning confocal microscope (LSM510; Carl Zeiss, Inc.; Fig. 10, A and F; and Fig. S4) or an epifluorescence microscope (TE2000U; Fig. 10 C). Epifluorescent image stacks were then deconvolved using the blind PSF algorithm (10 iterations) in AutoquantX (Media Cybernectics). Images of EB1 and KIF17 in Fig. 3 A were processed using the unsharp mask function in MetaMorph with a 3-pixel kernel size and a scaling factor of 0.9.

Immunofluorescence staining

Cells were fixed in −20°C methanol (10 s for KIF17 staining, 1–2 min for all others) or in 2% paraformaldehyde followed by permeabilization in PBS with 0.1% Triton X-100 for 2 min. In Fig. 4 D, to reduce soluble, over-expressed KIF17, cells were pre-extracted for 45 s in PEM (100 mM Pipes, 2 mM EGTA, and 2 mM MgCl, pH 6.9) containing 0.1% Triton X-100 followed by fixation in −20°C methanol. KIF17 was detected with rabbit anti–human KIF17 IgG generated in the laboratory (see Production of anti–human KIF17 antibody). Other antibodies used were: mouse anti-EB1 (for MDCK: 1A11, Abcam; for Caco2: BD), mouse anti–β-tubulin (TUB2.1; Sigma-Aldrich), mouse anti-acetylated tubulin (611B1; Sigma-Aldrich), rat anti-tyrosinated (Tyr) tubulin (YL1/2), rabbit anti-APC (H290; Santa-Cruz Biotechnology, Inc.), mouse anti-GP114, mouse anti-GP135, anti-aPKC (C20; Santa Cruz Biotechnology, Inc.), ZO-1 (MAB1520; Millipore), and E-cadherin (610181; BD). Fluorescently conjugated secondary antibodies (AMCA, FITC, Cy3, and Cy5) were obtained from Jackson ImmunoResearch Laboratories, Inc.

Production of anti–human KIF17 antibody

A human KIF17-specific peptide GHLLGEQNYLPQEEP (amino acids 587–601 within the stalk domain) was coupled to keyhole limpet hemocyanin, and antisera were produced in two New Zealand white rabbits by Sigma-Aldrich.

IgG was precipitated in saturated ammonium sulfate, resuspended, and bound to protein A–Sepharose 4B (GE Healthcare). IgG was eluted with 100 mM glycine, pH 2.8, and dialyzed against TBS, pH 8.0. Affinity purified IgG was prepared using bacterially purified GST-KIF17-Stalk coupled to cyanogen-bromide agarose (Sigma-Aldrich). Specific IgG was eluted with 0.5M acetic acid, dialyzed against PBS, pH 7.2, and concentrated by vacuum dialysis. IgG and affinity-purified fractions immunoprecipitated a protein of ~150 kD from HEK293 and Caco2 cell lysates, and recognized over-expressed KIF17-FL, KIF17-S, and KIF17-FL[G754E]. Immunoreactivity on blots and in fixed cells could be competed away by preincubation with immunogenic peptide (Fig. S1).

Protein procedures

Cells were washed twice in PBS with 0.1 mM CaCl$_2$ and 1 mM MgCl$_2$ (PBS-CM), then lysed in lysis buffer (50 mM Hepes, 150 mM NaCl, 1.5 mM MgCl$_2$, 0.1 mM CaCl$_2$, 10% glycerol, and 1% Triton X-100, pH 7.5, with 1 mM PMSF and protease inhibitor cocktail [Roche]). Lysates were cleared by centrifugation (16,000 g, 20min at 4°C) before SDS-PAGE, immunoprecipitation, or GST pull-down. For immunoprecipitation, lysates were incubated with 1–5 µg IgG at 4°C overnight (endogenous immunoprecipitation) or for 3 h (immunoprecipitation of overexpressed proteins). Protein A–Sepharose 4B (100 µl of a 10% slurry) was added for 1 h. Immune complexes were recovered by centrifugation and washed 3× in lysis buffer. For pull-downs, lysates were incubated with purified GST fusion proteins produced in bacteria for 2 h at 4°C. Beads were harvested by centrifugation and washed 3× in lysis buffer. Samples were boiled in SDS sample buffer, separated by SDS-PAGE, and transferred to nitrocellulose. Rabbit anti–mouse KIF17 (Sigma-Aldrich) was incubated with nitrocellulose membranes at 4°C overnight and was used for immunoblotting. Rabbit anti–human KIF17 was used for immunoprecipitation (except to demonstrate antibody specificity; Fig. S1). Other antibodies used were: mouse anti–kinesin-2 (K2.4; Covance), rabbit anti-GFP (Novus Biologicals), mouse anti-GFP (clones 7.1 and 13.1; Roche), rabbit anti-myc (C10; Delta Biolabs), mouse anti-Myc (9B11; Cell Signaling Technology), and rat anti-HA (Roche). Fluorescent secondary antibodies to mouse, rabbit, and rat IgG (Rockland and Invitrogen) were incubated with membranes for 1 h at room temperature. Proteins were detected using the Odyssey infrared imaging system (Li-Cor Biosciences). HA-tagged KIF17-FL was produced by in vitro translation using the TNT-T7–coupled rabbit reticulocyte lysate kit (Promega).

Protein knockdown

EB1, IQGAP1, and control siRNAs (0.5–3 µg; Shanghai GenePharma Co.), and pSM2c retroviral shRNA vectors (Thermo Fisher Scientific) targeting KIF17 or KIF9 negative control (KIF9 is not expressed in epithelial cells; Jaulin et al., 2007) were introduced into cells using the Amaxa nucleofector. Two or three sequential electroporations were performed at 2–3 d intervals. Cells were used 2 d after the final transfection. pGIPZ lentiviral shRNAs targeting KIF17 and pLKO.1 lentiviral control plasmid (Thermo Fisher Scientific) were introduced into cells by viral transduction. Lentiviral particles were produced in HEK293T cells as recommended by the manufacturer using pCMV-VSVG as a packaging plasmid. Viral particles were harvested, concentrated, and supplemented with 10 µg/µl polybrene just before cell transduction. MDCK and Caco2 cells were cultured with 4 and 15 µg/ml puromycin, respectively, after retroviral transfection or lentiviral transduction and used 4–8 d later. Both shKIF17#1 and shKIF17#2 reduce KIF17 protein levels in Caco2 cells. Only shKIF17#1 reduced KIF17 levels in MDCK cells. Retroviral shRNAs targeting KIF17 were used in experiments shown in Fig. 6. Lentiviral shRNAs were used in all other experiments shown. Although both retroviral and lentiviral KIF17 shRNAs gave similar results, lentiviral vectors were more effective at depleting KIF17.

siRNAs and shRNAs

siRNA TTGCCTTGAAGAAAGTGAA was used to target EB1 (Louie et al., 2004). siRNA negative control was 5'-UUCUCCGAACGUGUCACGUTT-3'. Retroviral and lentiviral shRNAs were obtained from Thermo Fisher Scientific. Lentiviral shRNAs in pGIPZ vector targeting KIF17 were: shKIF17#1, 5'-CCCACGTCACCGAGCAGATCA-3'; and shKIF17#2, 5'-ACCGGCT-GAAAGCCGACTATAA-3'. pLKO.1-puro was used as a control. Retroviral shRNA targeting KIF17 (also shKIF17#1) contains the same targeting sequence as in lentiviral shKIF17#1 but in the pSM2c expression vector. Retroviral pSM2c shRNA targeting KIF9 was 5'-AAAGCATTGATATTCACTTAAA-3'.

Online supplemental material

Fig. S1 shows characterization of KIF17 IgG, and KIF17 interaction with EB1 and KIF17[G754E]. Fig. S2 shows that KIF17[G754E-G243A] and KIF17[G754E-R288/294A] inhibit APC localization at MT plus ends. Fig. S3 shows that KIF17[G754E-G243A]

and KIF17$^{G754E\text{-}R288/294A}$ do not increase MT acetylation or stabilization. Fig. S4 shows that KIF17 silencing in Caco2 cells decreases the acetylated tubulin level and inhibits apical polarization. Video 1 shows time-lapse imaging of GFP-KIF17-FL in MDCK cells. Video 2 shows time-lapse imaging of GFP-KIF17^{G754E} in Caco2 cells. Online supplemental material is available at http://www.jcb.org/cgi/content/full/jcb.201006044/DC1.

References

Akhmanova, A., and M.O. Steinmetz. 2008. Tracking the ends: a dynamic protein network controls the fate of microtubule tips. *Nat. Rev. Mol. Cell Biol.* 9:309–322. doi:10.1038/nrm2369

Askham, J.M., P. Moncur, A.F. Markham, and E.E. Morrison. 2000. Regulation and function of the interaction between the APC tumour suppressor protein and EB1. *Oncogene.* 19:1950–1958. doi:10.1038/sj.onc.1203498

Bacallao, R., C. Antony, C. Dotti, E. Karsenti, E.H. Stelzer, and K. Simons. 1989. The subcellular organization of Madin-Darby canine kidney cells during the formation of a polarized epithelium. *J. Cell Biol.* 109:2817–2832. doi:10.1083/jcb.109.6.2817

Bieling, P., L. Laan, H. Schek, E.L. Munteanu, L. Sandblad, M. Dogterom, D. Brunner, and T. Surrey. 2007. Reconstitution of a microtubule plus-end tracking system in vitro. *Nature.* 450:1100–1105. doi:10.1038/nature06386

Bré, M.H., T.E. Kreis, and E. Karsenti. 1987. Control of microtubule nucleation and stability in Madin-Darby canine kidney cells: the occurrence of noncentrosomal, stable detyrosinated microtubules. *J. Cell Biol.* 105:1283–1296. doi:10.1083/jcb.105.3.1283

Browning, H., and D.D. Hackney. 2005. The EB1 homolog Mal3 stimulates the ATPase of the kinesin Tea2 by recruiting it to the microtubule. *J. Biol. Chem.* 280:12299–12304. doi:10.1074/jbc.M413620200

Browning, H., J. Hayles, J. Mata, L. Aveline, P. Nurse, and J.R. McIntosh. 2000. Tea2p is a kinesin-like protein required to generate polarized growth in fission yeast. *J. Cell Biol.* 151:15–28. doi:10.1083/jcb.151.1.15

Browning, H., D.D. Hackney, and P. Nurse. 2003. Targeted movement of cell end factors in fission yeast. *Nat. Cell Biol.* 5:812–818. doi:10.1038/ncb1034

Bu, W., and L.K. Su. 2003. Characterization of functional domains of human EB1 family proteins. *J. Biol. Chem.* 278:49721–49731. doi:10.1074/jbc.M306194200

Busch, K.E., J. Hayles, P. Nurse, and D. Brunner. 2004. Tea2p kinesin is involved in spatial microtubule organization by transporting tip1p on microtubules. *Dev. Cell.* 6:831–843. doi:10.1016/j.devcel.2004.05.008

Cai, D., D.P. McEwen, J.R. Martens, E. Meyhofer, and K.J. Verhey. 2009. Single molecule imaging reveals differences in microtubule track selection between kinesin motors. *PLoS Biol.* 7:e1000216. doi:10.1371/journal.pbio.1000216

Carvalho, P., M.L. Gupta Jr., M.A. Hoyt, and D. Pellman. 2004. Cell cycle control of kinesin-mediated transport of Bik1 (CLIP-170) regulates microtubule stability and dynein activation. *Dev. Cell.* 6:815–829. doi:10.1016/j.devcel.2004.05.001

Chausovsky, A., A.D. Bershadsky, and G.G. Borisy. 2000. Cadherin-mediated regulation of microtubule dynamics. *Nat. Cell Biol.* 2:797–804. doi:10.1038/35041037

Chu, P.J., J.F. Rivera, and D.B. Arnold. 2006. A role for Kif17 in transport of Kv4.2. *J. Biol. Chem.* 281:365–373. doi:10.1074/jbc.M508897200

Cohen, D., P.J. Brennwald, E. Rodriguez-Boulan, and A. Müsch. 2004. Mammalian PAR-1 determines epithelial lumen polarity by organizing the microtubule cytoskeleton. *J. Cell Biol.* 164:717–727. doi:10.1083/jcb.200308104

Cox, D.N., B. Lu, T.Q. Sun, L.T. Williams, and Y.N. Jan. 2001. *Drosophila* par-1 is required for oocyte differentiation and microtubule organization. *Curr. Biol.* 11:75–87. doi:10.1016/S0960-9822(01)00027-6

Coy, D.L., W.O. Hancock, M. Wagenbach, and J. Howard. 1999. Kinesin's tail domain is an inhibitory regulator of the motor domain. *Nat. Cell Biol.* 1:288–292. doi:10.1038/13001

Diamantopoulos, G.S., F. Perez, H.V. Goodson, G. Batelier, R. Melki, T.E. Kreis, and J.E. Rickard. 1999. Dynamic localization of CLIP-170 to microtubule plus ends is coupled to microtubule assembly. *J. Cell Biol.* 144:99–112. doi:10.1083/jcb.144.1.99

Dixit, R., B. Barnett, J.E. Lazarus, M. Tokito, Y.E. Goldman, and E.L. Holzbaur. 2009. Microtubule plus-end tracking by CLIP-170 requires EB1. *Proc. Natl. Acad. Sci. USA.* 106:492–497. doi:10.1073/pnas.0807614106

Doerflinger, H., R. Benton, J.M. Shulman, and D. St Johnston. 2003. The role of PAR-1 in regulating the polarised microtubule cytoskeleton in the *Drosophila* follicular epithelium. *Development.* 130:3965–3975. doi:10.1242/dev.00616

Dunn, S., E.E. Morrison, T.B. Liverpool, C. Molina-París, R.A. Cross, M.C. Alonso, and M. Peckham. 2008. Differential trafficking of Kif5c on tyrosinated and detyrosinated microtubules in live cells. *J. Cell Sci.* 121:1085–1095. doi:10.1242/jcs.026492

Eilers, U., J. Klumperman, and H.P. Hauri. 1989. Nocodazole, a microtubule-active drug, interferes with apical protein delivery in cultured intestinal epithelial cells (Caco-2). *J. Cell Biol.* 108:13–22. doi:10.1083/jcb.108.1.13

Elbert, M., D. Cohen, and A. Müsch. 2006. PAR1b promotes cell-cell adhesion and inhibits dishevelled-mediated transformation of Madin-Darby canine kidney cells. *Mol. Biol. Cell.* 17:3345–3355. doi:10.1091/mbc.E06-03-0193

Ferrari, A., A. Veligodskiy, U. Berge, M.S. Lucas, and R. Kroschewski. 2008. ROCK-mediated contractility, tight junctions and channels contribute to the conversion of a preapical patch into apical surface during isochoric lumen initiation. *J. Cell Sci.* 121:3649–3663. doi:10.1242/jcs.018648

Folker, E.S., B.M. Baker, and H.V. Goodson. 2005. Interactions between CLIP-170, tubulin, and microtubules: implications for the mechanism of Clip-170 plus-end tracking behavior. *Mol. Biol. Cell.* 16:5373–5384. doi:10.1091/mbc.E04-12-1106

Friedman, D.S., and R.D. Vale. 1999. Single-molecule analysis of kinesin motility reveals regulation by the cargo-binding tail domain. *Nat. Cell Biol.* 1:293–297. doi:10.1038/13008

Fukata, M., M. Nakagawa, N. Itoh, A. Kawajiri, M. Yamaga, S. Kuroda, and K. Kaibuchi. 2001. Involvement of IQGAP1, an effector of Rac1 and Cdc42 GTPases, in cell-cell dissociation during cell scattering. *Mol. Cell. Biol.* 21:2165–2183. doi:10.1128/MCB.21.6.2165-2183.2001

Fukata, M., T. Watanabe, J. Noritake, M. Nakagawa, M. Yamaga, S. Kuroda, Y. Matsuura, A. Iwamatsu, F. Perez, and K. Kaibuchi. 2002. Rac1 and Cdc42 capture microtubules through IQGAP1 and CLIP-170. *Cell.* 109:873–885. doi:10.1016/S0092-8674(02)00800-0

Galjart, N. 2005. CLIPs and CLASPs and cellular dynamics. *Nat. Rev. Mol. Cell Biol.* 6:487–498. doi:10.1038/nrm1664

Gilbert, T., A. Le Bivic, A. Quaroni, and E. Rodriguez-Boulan. 1991. Microtubular organization and its involvement in the biogenetic pathways of plasma membrane proteins in Caco-2 intestinal epithelial cells. *J. Cell Biol.* 113:275–288. doi:10.1083/jcb.113.2.275

Guillaud, L., M. Setou, and N. Hirokawa. 2003. KIF17 dynamics and regulation of NR2B trafficking in hippocampal neurons. *J. Neurosci.* 23:131–140.

Hayashi, I., A. Wilde, T.K. Mal, and M. Ikura. 2005. Structural basis for the activation of microtubule assembly by the EB1 and p150Glued complex. *Mol. Cell.* 19:449–460. doi:10.1016/j.molcel.2005.06.034

Honnappa, S., S.M. Gouveia, A. Weisbrich, F.F. Damberger, N.S. Bhavesh, H. Jawhari, I. Grigoriev, F.J. van Rijssel, R.M. Buey, A. Lawera, et al. 2009. An EB1-binding motif acts as a microtubule tip localization signal. *Cell.* 138:366–376. doi:10.1016/j.cell.2009.04.065

Huyett, A., J. Kahana, P. Silver, X. Zeng, and W.S. Saunders. 1998. The Kar3p and Kip2p motors function antagonistically at the spindle poles to influence cytoplasmic microtubule numbers. *J. Cell Sci.* 111:295–301.

Ikegami, K., R.L. Heier, M. Taruishi, H. Takagi, M. Mukai, S. Shimma, S. Taira, K. Hatanaka, N. Morone, I. Yao, et al. 2007. Loss of alpha-tubulin polyglutamylation in ROSA22 mice is associated with abnormal targeting of KIF1A and modulated synaptic function. *Proc. Natl. Acad. Sci. USA.* 104:3213–3218. doi:10.1073/pnas.0611547104

Imanishi, M., N.F. Endres, A. Gennerich, and R.D. Vale. 2006. Autoinhibition regulates the motility of the *C. elegans* intraflagellar transport motor OSM-3. *J. Cell Biol.* 174:931–937. doi:10.1083/jcb.200605179

Infante, A.S., M.S. Stein, Y. Zhai, G.G. Borisy, and G.G. Gundersen. 2000. Detyrosinated (Glu) microtubules are stabilized by an ATP-sensitive plus-end cap. *J. Cell Sci.* 113:3907–3919.

Insinna, C., N. Pathak, B. Perkins, I. Drummond, and J.C. Besharse. 2008. The homodimeric kinesin, Kif17, is essential for vertebrate photoreceptor sensory outer segment development. *Dev. Biol.* 316:160–170. doi:10.1016/j.ydbio.2008.01.025

Jaulin, F., X. Xue, E. Rodriguez-Boulan, and G. Kreitzer. 2007. Polarization-dependent selective transport to the apical membrane by KIF5B in MDCK cells. *Dev. Cell.* 13:511–522. doi:10.1016/j.devcel.2007.08.001

Jenkins, P.M., T.W. Hurd, L. Zhang, D.P. McEwen, R.L. Brown, B. Margolis, K.J. Verhey, and J.R. Martens. 2006. Ciliary targeting of olfactory CNG channels requires the CNGB1b subunit and the kinesin-2 motor protein, KIF17. *Curr. Biol.* 16:1211–1216. doi:10.1016/j.cub.2006.04.034

Jimbo, T., Y. Kawasaki, R. Koyama, R. Sato, S. Takada, K. Haraguchi, and T. Akiyama. 2002. Identification of a link between the tumour suppressor APC and the kinesin superfamily. *Nat. Cell Biol.* 4:323–327. doi:10.1038/ncb779

Khawaja, S., G.G. Gundersen, and J.C. Bulinski. 1988. Enhanced stability of microtubules enriched in detyrosinated tubulin is not a direct function of detyrosination level. *J. Cell Biol.* 106:141–149. doi:10.1083/jcb.106.1.141

Kita, K., T. Wittmann, I.S. Näthke, and C.M. Waterman-Storer. 2006. Adenomatous polyposis coli on microtubule plus ends in cell extensions can promote microtubule net growth with or without EB1. *Mol. Biol. Cell.* 17:2331–2345. doi:10.1091/mbc.E05-06-0498

Kodama, A., I. Karakesisoglou, E. Wong, A. Vaezi, and E. Fuchs. 2003. ACF7: an essential integrator of microtubule dynamics. *Cell.* 115:343–354. doi:10.1016/S0092-8674(03)00813-4

Komarova, Y., G. Lansbergen, N. Galjart, F. Grosveld, G.G. Borisy, and A. Akhmanova. 2005. EB1 and EB3 control CLIP dissociation from the ends of growing microtubules. *Mol. Biol. Cell.* 16:5334–5345. doi:10.1091/mbc.E05-07-0614

Konishi, Y., and M. Setou. 2009. Tubulin tyrosination navigates the kinesin-1 motor domain to axons. *Nat. Neurosci.* 12:559–567. doi:10.1038/nn.2314

Konzack, S., P.E. Rischitor, C. Enke, and R. Fischer. 2005. The role of the kinesin motor KipA in microtubule organization and polarized growth of *Aspergillus nidulans. Mol. Biol. Cell.* 16:497–506. doi:10.1091/mbc.E04-02-0083

Kreitzer, G., G. Liao, and G.G. Gundersen. 1999. Detyrosination of tubulin regulates the interaction of intermediate filaments with microtubules in vivo via a kinesin-dependent mechanism. *Mol. Biol. Cell.* 10:1105–1118.

Kroboth, K., I.P. Newton, K. Kita, D. Dikovskaya, J. Zumbrunn, C.M. Waterman-Storer, and I.S. Näthke. 2007. Lack of adenomatous polyposis coli protein correlates with a decrease in cell migration and overall changes in microtubule stability. *Mol. Biol. Cell.* 18:910–918. doi:10.1091/mbc.E06-03-0179

Lee, J.R., H. Shin, J. Choi, J. Ko, S. Kim, H.W. Lee, K. Kim, S.H. Rho, J.H. Lee, H.E. Song, et al. 2004. An intramolecular interaction between the FHA domain and a coiled coil negatively regulates the kinesin motor KIF1A. *EMBO J.* 23:1506–1515. doi:10.1038/sj.emboj.7600164

Liao, G., and G.G. Gundersen. 1998. Kinesin is a candidate for cross-bridging microtubules and intermediate filaments. Selective binding of kinesin to detyrosinated tubulin and vimentin. *J. Biol. Chem.* 273:9797–9803. doi:10.1074/jbc.273.16.9797

Ligon, L.A., S.S. Shelly, M. Tokito, and E.L. Holzbaur. 2003. The microtubule plus-end proteins EB1 and dynactin have differential effects on microtubule polymerization. *Mol. Biol. Cell.* 14:1405–1417. doi:10.1091/mbc.E02-03-0155

Lin, S.X., G.G. Gundersen, and F.R. Maxfield. 2002. Export from pericentriolar endocytic recycling compartment to cell surface depends on stable, detyrosinated (glu) microtubules and kinesin. *Mol. Biol. Cell.* 13:96–109. doi:10.1091/mbc.01-05-0224

Louie, R.K., S. Bahmanyar, K.A. Siemers, V. Votin, P. Chang, T. Stearns, W.J. Nelson, and A.I. Barth. 2004. Adenomatous polyposis coli and EB1 localize in close proximity of the mother centriole and EB1 is a functional component of centrosomes. *J. Cell Sci.* 117:1117–1128. doi:10.1242/jcs.00939

Matter, K., K. Bucher, and H.P. Hauri. 1990. Microtubule perturbation retards both the direct and the indirect apical pathway but does not affect sorting of plasma membrane proteins in intestinal epithelial cells (Caco-2). *EMBO J.* 9:3163–3170.

Meder, D., A. Shevchenko, K. Simons, and J. Füllekrug. 2005. Gp135/podocalyxin and NHERF-2 participate in the formation of a preapical domain during polarization of MDCK cells. *J. Cell Biol.* 168:303–313. doi:10.1083/jcb.200407072

Mimori-Kiyosue, Y., N. Shiina, and S. Tsukita. 2000a. Adenomatous polyposis coli (APC) protein moves along microtubules and concentrates at their growing ends in epithelial cells. *J. Cell Biol.* 148:505–518. doi:10.1083/jcb.148.3.505

Mimori-Kiyosue, Y., N. Shiina, and S. Tsukita. 2000b. The dynamic behavior of the APC-binding protein EB1 on the distal ends of microtubules. *Curr. Biol.* 10:865–868. doi:10.1016/S0960-9822(00)00600-X

Minin, A.A. 1997. Dispersal of Golgi apparatus in nocodazole-treated fibroblasts is a kinesin-driven process. *J. Cell Sci.* 110:2495–2505.

Müsch, A. 2004. Microtubule organization and function in epithelial cells. *Traffic.* 5:1–9. doi:10.1111/j.1600-0854.2003.00149.x

Nakata, T., and N. Hirokawa. 2003. Microtubules provide directional cues for polarized axonal transport through interaction with kinesin motor head. *J. Cell Biol.* 162:1045–1055. doi:10.1083/jcb.200302175

Näthke, I.S., C.L. Adams, P. Polakis, J.H. Sellin, and W.J. Nelson. 1996. The adenomatous polyposis coli tumor suppressor protein localizes to plasma membrane sites involved in active cell migration. *J. Cell Biol.* 134:165–179. doi:10.1083/jcb.134.1.165

O'Brien, L.E., W. Yu, K. Tang, T.S. Jou, M.M. Zegers, and K.E. Mostov. 2006. Morphological and biochemical analysis of Rac1 in three-dimensional epithelial cell cultures. *Methods Enzymol.* 406:676–691. doi:10.1016/S0076-6879(06)06053-8

Pepperkok, R., M.H. Bré, J. Davoust, and T.E. Kreis. 1990. Microtubules are stabilized in confluent epithelial cells but not in fibroblasts. *J. Cell Biol.* 111:3003–3012. doi:10.1083/jcb.111.6.3003

Piperno, G., M. LeDizet, and X.J. Chang. 1987. Microtubules containing acetylated α-tubulin in mammalian cells in culture. *J. Cell Biol.* 104:289–302. doi:10.1083/jcb.104.2.289

Reed, N.A., D. Cai, T.L. Blasius, G.T. Jih, E. Meyhofer, J. Gaertig, and K.J. Verhey. 2006. Microtubule acetylation promotes kinesin-1 binding and transport. *Curr. Biol.* 16:2166–2172. doi:10.1016/j.cub.2006.09.014

Rindler, M.J., I.E. Ivanov, and D.D. Sabatini. 1987. Microtubule-acting drugs lead to the nonpolarized delivery of the influenza hemagglutinin to the cell surface of polarized Madin-Darby canine kidney cells. *J. Cell Biol.* 104:231–241. doi:10.1083/jcb.104.2.231

Rowan, A.J., H. Lamlum, M. Ilyas, J. Wheeler, J. Straub, A. Papadopoulou, D. Bicknell, W.F. Bodmer, and I.P. Tomlinson. 2000. APC mutations in sporadic colorectal tumors: A mutational "hotspot" and interdependence of the "two hits". *Proc. Natl. Acad. Sci. USA.* 97:3352–3357. doi:10.1073/pnas.97.7.3352

Salaycik, K.J., C.J. Fagerstrom, K. Murthy, U.S. Tulu, and P. Wadsworth. 2005. Quantification of microtubule nucleation, growth and dynamics in wound-edge cells. *J. Cell Sci.* 118:4113–4122. doi:10.1242/jcs.02531

Sandblad, L., K.E. Busch, P. Tittmann, H. Gross, D. Brunner, and A. Hoenger. 2006. The *Schizosaccharomyces pombe* EB1 homolog Mal3p binds and stabilizes the microtubule lattice seam. *Cell.* 127:1415–1424. doi:10.1016/j.cell.2006.11.025

Saunders, C., and L.E. Limbird. 1997. Disruption of microtubules reveals two independent apical targeting mechanisms for G-protein-coupled receptors in polarized renal epithelial cells. *J. Biol. Chem.* 272:19035–19045. doi:10.1074/jbc.272.30.19035

Setou, M., T. Nakagawa, D.H. Seog, and N. Hirokawa. 2000. Kinesin superfamily motor protein KIF17 and mLin-10 in NMDA receptor-containing vesicle transport. *Science.* 288:1796–1802. doi:10.1126/science.288.5472.1796

Sharma, M., L. Leung, M. Brocardo, J. Henderson, C. Flegg, and B.R. Henderson. 2006. Membrane localization of adenomatous polyposis coli protein at cellular protrusions: targeting sequences and regulation by beta-catenin. *J. Biol. Chem.* 281:17140–17149. doi:10.1074/jbc.M513027200

Skube, S.B., J.M. Chaverri, and H.V. Goodson. 2010. Effect of GFP tags on the localization of EB1 and EB1 fragments in vivo. *Cytoskeleton (Hoboken).* 67:1–12.

Slep, K.C., S.L. Rogers, S.L. Elliott, H. Ohkura, P.A. Kolodziej, and R.D. Vale. 2005. Structural determinants for EB1-mediated recruitment of APC and spectraplakins to the microtubule plus end. *J. Cell Biol.* 168:587–598. doi:10.1083/jcb.200410114

Snow, J.J., G. Ou, A.L. Gunnarson, M.R. Walker, H.M. Zhou, I. Brust-Mascher, and J.M. Scholey. 2004. Two anterograde intraflagellar transport motors cooperate to build sensory cilia on *C. elegans* neurons. *Nat. Cell Biol.* 6:1109–1113. doi:10.1038/ncb1186

Verhey, K.J., and J. Gaertig. 2007. The tubulin code. *Cell Cycle.* 6:2152–2160.

Vitre, B., F.M. Coquelle, C. Heichette, C. Garnier, D. Chrétien, and I. Arnal. 2008. EB1 regulates microtubule dynamics and tubulin sheet closure in vitro. *Nat. Cell Biol.* 10:415–421. doi:10.1038/ncb1703

Wang, X., and T.L. Schwarz. 2009. The mechanism of Ca2+ -dependent regulation of kinesin-mediated mitochondrial motility. *Cell.* 136:163–174. doi:10.1016/j.cell.2008.11.046

Watanabe, T., S. Wang, J. Noritake, K. Sato, M. Fukata, M. Takefuji, M. Nakagawa, N. Izumi, T. Akiyama, and K. Kaibuchi. 2004. Interaction with IQGAP1 links APC to Rac1, Cdc42, and actin filaments during cell polarization and migration. *Dev. Cell.* 7:871–883. doi:10.1016/j.devcel.2004.10.017

Waterman-Storer, C.M., W.C. Salmon, and E.D. Salmon. 2000. Feedback interactions between cell-cell adherens junctions and cytoskeletal dynamics in newt lung epithelial cells. *Mol. Biol. Cell.* 11:2471–2483.

Webster, D.R., and G.G. Borisy. 1989. Microtubules are acetylated in domains that turn over slowly. *J. Cell Sci.* 92:57–65.

Webster, D.R., G.G. Gundersen, J.C. Bulinski, and G.G. Borisy. 1987. Differential turnover of tyrosinated and detyrosinated microtubules. *Proc. Natl. Acad. Sci. USA.* 84:9040–9044. doi:10.1073/pnas.84.24.9040

Wen, Y., C.H. Eng, J. Schmoranzer, N. Cabrera-Poch, E.J. Morris, M. Chen, B.J. Wallar, A.S. Alberts, and G.G. Gundersen. 2004. EB1 and APC bind to mDia to stabilize microtubules downstream of Rho and promote cell migration. *Nat. Cell Biol.* 6:820–830. doi:10.1038/ncb1160

Witte, H., D. Neukirchen, and F. Bradke. 2008. Microtubule stabilization specifies initial neuronal polarization. *J. Cell Biol.* 180:619–632. doi:10.1083/jcb.200707042

Woehlke, G., A.K. Ruby, C.L. Hart, B. Ly, N. Hom-Booher, and R.D. Vale. 1997. Microtubule interaction site of the kinesin motor. *Cell.* 90:207–216. doi:10.1016/S0092-8674(00)80329-3

Wu, X., X. Xiang, and J.A. Hammer III. 2006. Motor proteins at the microtubule plus-end. *Trends Cell Biol.* 16:135–143. doi:10.1016/j.tcb.2006.01.004

Zumbrunn, J., K. Kinoshita, A.A. Hyman, and I.S. Näthke. 2001. Binding of the adenomatous polyposis coli protein to microtubules increases microtubule stability and is regulated by GSK3 beta phosphorylation. *Curr. Biol.* 11:44–49. doi:10.1016/S0960-9822(01)00002-1